

Article

Origin of Historical Ba-Rich Slags Related to Pb-Ag Production from Jihlava Ore District (Czech Republic)

Jaroslav Kapusta ^{1,2,*}, Zdeněk Dolníček ³, Ondra Sracek ¹ and Karel Malý ⁴

¹ Department of Geology, Faculty of Science, Palacký University, 17. Listopadu 1192/12, 771 46 Olomouc, Czech Republic; ondrej.sracek@upol.cz

² Department of Geological Sciences, Faculty of Science, Masaryk University, Kotlářská 2, 611 37 Brno, Czech Republic

³ Department of Mineralogy and Petrology, National Museum, Cirkusová 1740, 193 00 Prague 9-Horní Počernice, Czech Republic; zdenek.dolnicek@nm.cz

⁴ Vysočina Museum Jihlava, Masarykovo Náměstí 55, 586 01 Jihlava, Czech Republic; maly@muzeum.ji.cz

* Correspondence: jaroslav.kapusta@upol.cz

Abstract: The aim of this study was to characterize historical slags which originated during silver production from the Jihlava ore district, Czech Republic. The area was among the head producers of silver within the Lands of the Czech Crown in 13th–14th centuries. The mined ores had complex composition, being formed mostly by pyrite, sphalerite, galena, chalcopyrite, and accessory silver-rich minerals such as silver-bearing tetrahedrite (freibergite) or pyrargyrite, with gangue represented by quartz and Mn-rich carbonates or baryte. Large volumes of slags with contrasting composition were generated during the Pb-Ag production. Altogether, two main types of slags were identified in the district. The first type is characterized by high BaO contents (up to 34.5 wt.%) and dominance of glass, minor quartz, and accessory amounts of Ba-rich feldspar (up to 93 mol.% of Cls), metal-rich inclusions, Ba-Pb sulphates and only rare pyroxene, wollastonite and melilite. The composition of the second group belongs to fayalitic slags containing glass, Fe-rich olivine, accessory pyroxene, feldspar, quartz, and inclusions of various metallic phases. Fluxes were derived from gangue (quartz, carbonates, baryte) or local host rocks for both types of slag. The calculated viscosity indexes reflect (with minor exceptions) medium-to-high effectivity of metal separation. Smelting temperatures were estimated from a series of ternary plots; however, more reliable estimates for both types of slags were obtained only from experimental determination of melting temperature and calculations using bulk/glass compositions (~1100–1200 °C).

Keywords: slags; lead; silver; baryte; Jihlava Ore District; archaeometry; smelting

Citation: Kapusta, J.; Dolníček, Z.; Sracek, O.; Malý, K. Origin of Historical Ba-Rich Slags Related to Pb-Ag Production from Jihlava Ore District (Czech Republic). *Minerals* **2022**, *12*, 985. <https://doi.org/10.3390/min12080985>

Academic Editors: Gianni Gallelo and Marco Lezzerini

Received: 14 July 2022

Accepted: 28 July 2022

Published: 2 August 2022

Publisher's Note: MDPI stays neutral with regard to jurisdictional claims in published maps and institutional affiliations.



Copyright: © 2022 by the authors. Licensee MDPI, Basel, Switzerland. This article is an open access article distributed under the terms and conditions of the Creative Commons Attribution (CC BY) license (<https://creativecommons.org/licenses/by/4.0/>).

1. Introduction

Slag is defined as a solidified waste resulting from metal production or fuel combustion. In metallurgy, the key role of slag is protection of reduced metal from oxidation as well as waste elements fixation [1]. Only historical use of native metals and modern hydrometallurgy could be marked as slag-free metal yielding technology [2]. Up to date, there have been published numerous studies dealing with slags from base metal production and most of them could be divided into two main groups. The first one is related to recent metallurgy, where slags are perceived as waste; hence, the important topic is their utilization or reworking (e.g., [3]). The latter is the archaeological approach, which recognizes historical slags as an important source of information, because smelting methodology is imprinted into their composition. Additionally, slags are usually present in the order of magnitude of one hundred kilograms on a smelting site, and they last for centuries [1,4–13].

Both the modern and the historical slags are often subjects of hazard assessment studies due to their possible elevated contents of heavy metals and metalloids, which are predominantly fixed in glass and other phases vulnerable to dissolution [14–18].

The aim of this study is geochemical and mineralogical characterization of Ba-rich and fayalitic slags resulting from silver production in the Jihlava Ore District, including estimation of charge composition and smelting conditions. Part of the study is also the smelting temperature calculation and its verification using a series of experimental melting data.

2. History and Ore Mineralization of Studied Sites

2.1. Historical Background

The Jihlava Ore District (JOD) was one of the head silver producers in the Europe in the 13th century. However, the historical importance of the region also stems from the mining rights written back in 1249 AD [19]. The JOD, with its centre in Jihlava city, represents the origin of medieval silver mining in the Bohemian-Moravian Highlands. Jihlava is situated on the historical border between the Bohemian and the Moravian parts of the Czech Republic. The borderline is represented by the Jihlava River, which splits the city into two parts, northern and southern. The combination of a high altitude and the topographic situation together with harsh weather ruled out most of the agricultural effort in the area, and it is also the reason why Jihlava was only a small settlement in the pre-mining period [20,21]. This rapidly changed during the first period of mining in the area, which could be marked as the top of silver production in the JOD [22].

While there is a long-term debate regarding the time classification of the beginning of mining in the JOD, with a principal consensus on the third decade of 13th century, there is no doubt about the localization of the event within today's Jihlava city itself into its northwestern part called Staré Hory (in Latin antiquus mons = old mines) [23]. Surprisingly, the oldest reference directly related to the mining activity at the Staré Hory Dislocation (further in the text SHD) area comes from 1315 AD, whereas there are numerous mentions from the other medieval mining sites within the JOD dated back to the second half of the 13th century [19].

The JOD ores were exploited over seven centuries with two main interruptions coming from socio-economic factors: the Hussite wars in the first half of the 15th century, followed by famine and the devaluation of the silver market in Europe by the import of South American silver in the 17th century [22]. It is estimated that around 488 tons of silver were produced during the lifespan of mining in the district [24].

2.2. Ore Mineralization in the JOD

The Lower Permian hydrothermal Ag-Pb-Zn ore mineralization of the JOD is hosted by gneisses and migmatites of Monotonous and Variegated Groups of the Moldanubian Zone of the Bohemian Massif. The ore mineralization is located within the NNE-SSW and N-W fault zones, and is genetically bonded to granitic intrusions of the Moldanubian Batholith [22]. The longest mineralized NNE-SSW-oriented structure is the SHD Zone, which measures ~9 km and runs through the eastern part of Jihlava town and outcrops at several places (Figure 1) [22,25].

Over the years, various classifications of JOD hydrothermal mineralization have been proposed due to advances in analytical methods and knowledge of ore-forming processes [26,27]. The most comprehensive approach is presented in [22]. Authors divided the JOD mineralization into six individual groups based on mineral composition, sphalerite colouration, and mineral succession. The prevalent ore type is composed of pyrite, black sphalerite, galena, minor chalcopyrite, arsenopyrite, and tetrahedrite. Pyrrhotite and pyrrargyrite are only accessories. Gangue minerals are represented by quartz and carbonates (calcite, dolomite, and siderite) with notable contents of MnO (up to 26 wt.% of MnO in siderite) [28]. The temperature of ore formation is estimated from sulphur isotope

thermometry in the range of 350–450 °C [29]. There is historical significance to mineralization formed by galena, lightly coloured sphalerite, and only subordinate amounts of chalcopyrite and Ag-rich tetrahedrite (freibergite). Gangue is composed of several generations of quartz and tabular crystals of baryte [22]. Carbonates are rare, and their chemical composition corresponds to calcite with only minor admixtures represented mostly by Mn (~2 wt.% of MnO) [28]. The hydrothermal fluids had temperatures of around 250 °C, as indicated by the isotopic thermometer [29].

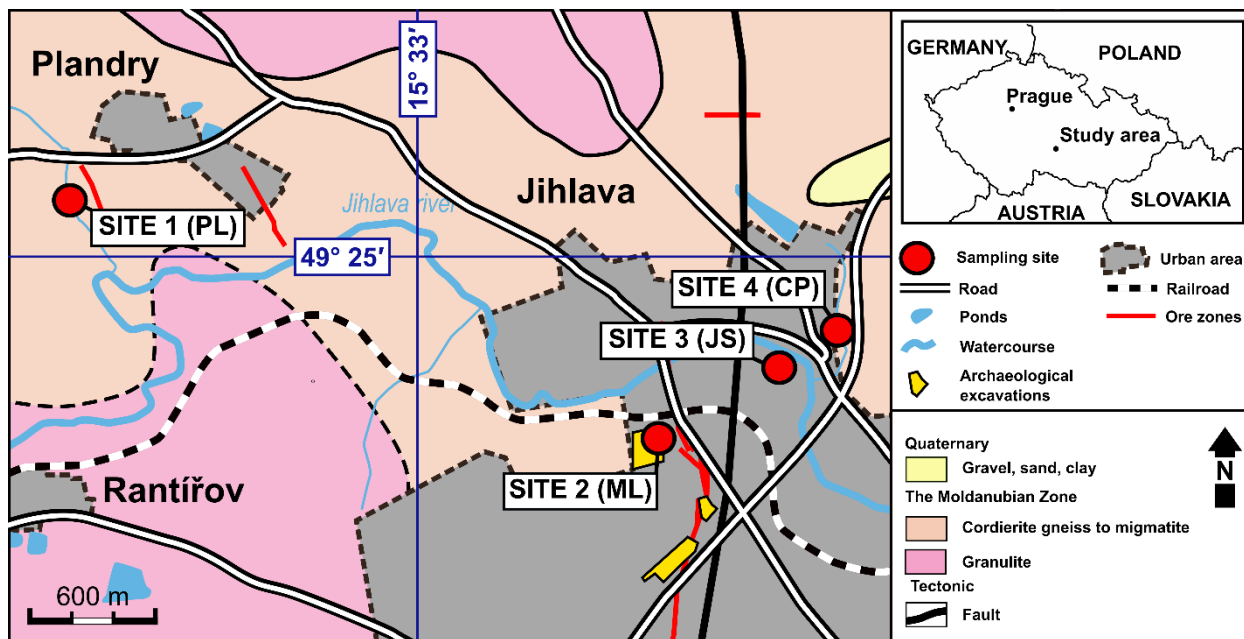


Figure 1. Localization of sampling sites. Archaeological excavations and outcropping ore mineralization are projected according to [30].

3. Studied Sites and Evidence of Metallurgical Activities

The slag samples come from four individual sites (Figure 1). All sites are closely associated with water courses since water was essential for ore processing and represented the main source of kinetic power for furnaces, bellows, and stamps in the Late Middle Ages and further on [31].

The first sampling site (Site 1, samples notation PL) lies in the valley of the Bělokamenský creek close to the Plandry village and approximately 5 km NW from the Jihlava city centre. The locality is nowadays forested, and its part is an artificial elevation with a round base, which represents the remains of a fortified defensive structure called the “motte” [32]. Previous archaeological surveys at the motte and surrounding trench yielded fragments of glazed pottery, two lead bullions, and minor iron objects (arrow heads, nails, and hinges) [33]. A slag heap is covered by a ~30 cm thick layer of soil, and slag material is observed only at the riverbank, where it reaches up to 0.5 m. The slags also represent a continuous infill of the riverbed in a total length of about 30 m downstream. Even though no remains of furnaces were identified on the locality so far [34], the number of produced slags in the magnitude of tonnes is good evidence of historical smelting activities. Two fragments of grinding stones carved out of granite were found immediately by the slag accumulation, indicating primary ore processing or mechanical milling of slags from previous smelting [35].

Two types of slags are found at the site. The first group (Type A) is represented by whole pieces and fragments up to 20 cm in size with a plane or elongated shape, and well-formed flow patterns on the top of some samples. The colour ranges from grey to dark grey, with a bluish tint, and dull to semi-metallic lustre. Weathered parts of the slags are either ochre or light grey in colour. Some samples exhibit a predominant concentration of

large pores (< 2 cm) as well as quartz grains near the upper surface. Additionally, olivine laths are sometimes visible on fracture planes and cuts. Small fragments of quartz and host rocks are usually embedded at the bottom surface of the samples (Figure 2, PL15). Macroscopically visible inclusions of matte (mixture of sulphides) and reduced metals (a few millimetres in size) are randomly scattered within the samples.

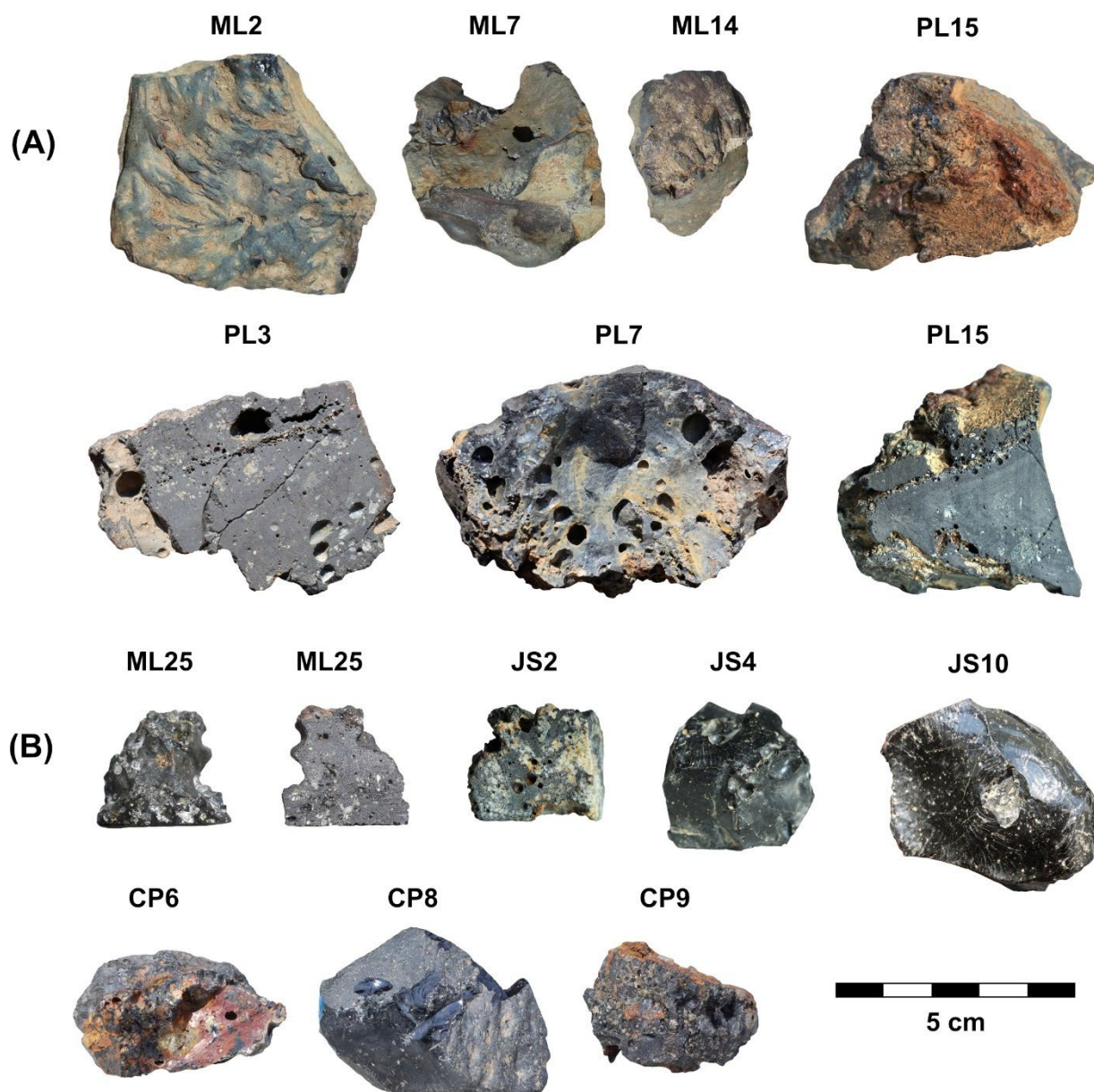


Figure 2. Macrophotographs of Type (A) slags from Sites 1 and 2 and Type (B) slags from Sites 2, 3, and 4.

A single slag fragment (Type B) deviates from the above-mentioned group by its black colour and glassy lustre. The shape of the sample is isometric and overall size is approximately 6 cm. Thin shards have a dark green colour, and the pulverized sample is grey. The sample is almost free of pores and macroscopically visible inclusions of quartz or metals in any form (matte, metallic alloys, etc.).

Sites 2, 3, and 4 (samples notation ML, JS, and CP, respectively) are located in the northwestern part of the city of Jihlava and are closely related to the SHD area and the longest mineralized structure in the district. The SHD area was the subject of extensive

rescue archaeological excavations in the past (2001–2006, 2014, and 2016), which resulted in about 5 ha of exposed area. The surveys led to discovery of ore-processing structures, vertical mining shafts, mill stones, lead bullion, and notable amount of iron tools [36] as well as pottery and technical ceramics [37], and, last but not least, the remains of the mining settlement [20,38]. According to archaeological findings, the main role of the area was mining and ore processing and only marginally base metal smelting [36]. Therefore, the slags are relatively scarce in the locality. The slags were found mostly on the riverbanks (Site 3 and 4), but also as an infill of the processing structures (Site 2). The slag categorization proposed for Site 1 also applies to SHD sites with some minor differences and exceptions. The Type A samples are made by slags greenish to bluish in colour, often with distinctive flow patterns on the preserved upper surface and dull lustre. Most of the samples have plane shape with thickness up to 4 cm and overall size not exceeding 8 cm; the rest are smaller fragments. Some slags are partially ochre-coloured by iron oxy-hydroxides, which are also present as an impregnation on cracks. The colour on a freshly cut surface is dark grey with a blueish tint. The slags contain partially melted white fragments of quartz, which are usually randomly distributed within a sample, but sometimes are arranged into a layer near the top surface of the slag (best observable on the vertically oriented cuts, Figure 2). Inclusions of matte and metals are accessory, and they are easily recognizable on fresh cuts and fracture planes due to their bright metallic lustre and oval-to-round shape. Their size is usually in the range of first millimetres with maximum of about 6 mm. The slags contain fewer pores in comparison with similar material from Site 1.

The second group (Type B) of slags consists of black-coloured fragments up to 6 cm in size. The overall shape of these slags is mostly isometric, occasionally elongated, with clearly visible fractures. They are also prone to cracking upon cutting. Slags have a glassy lustre, sometimes with distinctive iridescence resembling old weathered glass. A significant amount of unreacted quartz grains is a common part of some samples (e.g., Figure 2, JS2). Macroscopically visible pores and inclusions of metals and matte are rather scarce.

The Type B slags are present at all localities; the Type A slags were found exclusively at Sites 1 and 2.

4. Materials and Methods

4.1. Slag Selection and Preparation

All slags were preliminarily screened by the handheld ED-XRF Delta Premium device. The results, together with macroscopic features, were used for the selection of representative samples for following analytical methods ($n = 37$). A small part of each slag sample was separated by diamond saw, mounted into epoxy resin, and polished. The cut-outs were used for pycnometric determination of density. The scraps (~30 g from each sample) were pulverized in a puck mill and used for XRD and bulk chemical analyses. The inclusions of quartz, metals, sulphides, and matte were not removed prior to the grinding.

4.2. Optical Microscopy and Electron Microprobe

The polished thin sections were examined under polarizing microscope Olympus BX50-p in transmitted and reflected light. Composition of selected phases was determined using wavelength dispersive spectrometry on Cameca SX-100 microprobe (National Museum, Prague, Czech Republic) and energy dispersive spectrometry on Jeol-JXA 8600 microprobe at the Department of Geology, Palacký University Olomouc, Czech Republic. Silicates, glass, and sulphates were analysed under following conditions: accelerating voltage 15 kV, probe current 10 nA, beam diameter 1–5 μm , and counting time 10 s (60 s for EDS). The following set of standards was used for the quantification of obtained raw data: sanidine (Si, Al, K), diopside (Mg), albite (Na), apatite (P), wollastonite (Si, Ca), celestine (S, Sr), rhodonite (Mn), vanadinite (Pb), baryte (Ba), haematite (Fe), ZnO (Zn),

chalcopyrite (Cu), RbGe glass (Rb), Cs glass (Cs), TiO₂ (Ti), vanadium metal (V), and Cr₂O₃ (Cr).

4.3. Bulk Chemical Analyses

Some chemical analyses ($n = 18$) were executed at the ACME laboratories in Vancouver, Canada. Sulphur and carbon were analysed by LECO. Major oxides and trace elements were determined by the combination of ICP-OES (Spectro Ciros Vision) and ICP-MS (PerkinElmer ELAN 9000) method following (1) fusion with lithium metaborate/tetraborate flux and digestion in nitric acid (ICP-OES, ICP-MS) and (2) aqua regia digestion (ICP-MS, precious and base metals). Contents that exceeded the upper limit of the analytical method (high contents of Zn, Pb, and Ba) were further analysed by Solaar M5 TJA Solutions atomic absorption spectroscopy at the Department of Geological Sciences in Brno, Czech Republic. The remaining ($n = 19$) of slags were analysed at the Department of Geology, Palacký University Olomouc, Czech Republic, by WD-XRF method (S4 PIONEER). The measurements were carried out on 40 mm diameter discs pressed from samples mixed with microcrystalline cellulose in ratio 4:1 under pressure of 20 tons.

4.4. X-ray Powder Diffraction

Selected powdered samples were analysed by Bruker-AXS D8 X-ray powder diffraction equipped with silicon stripped detector LynxEye under following conditions: CuK α /Ni radiation, voltage 40 kV, current 40 mA, and step 0.014° 2 θ with counting time 15 s in position. The acquired diffraction records were evaluated by EVA software and PDF-2 database. The Rietveld refinement in combination with TOPAS software (v. 4.2 Bruker) was used for estimation of semi-quantitative composition of the samples.

4.5. Determination of Smelting Temperature

The liquidus temperatures were calculated from bulk and glass chemical composition using Melts software (rhyolite-MELTS_v1.0.x). The selected conditions were: atmospheric pressure (0.1 mPa) and QFM oxygen buffer. The melting points of the slags were also determined by stepped heating under the reducing atmosphere. The samples were cut into small slabs and placed on coasters measuring ca. 35 mm \times 50 mm cut from fireclay. The whole assembly was placed on a silica refractory brick and placed in a muffle furnace (LM312.11). The samples were gradually exposed to temperatures of 1000 °C, 1050 °C, 1100 °C, 1150 °C, and 1200 °C, lasting 1 h each. The reducing atmosphere during the tests was achieved by filling the remaining volume of the furnace with charcoal.

5. Results

5.1. Bulk Chemical Composition

The bulk chemical composition of studied slags is presented in Table 1. All the samples are silicate-based (38.3–59.4 wt.% of SiO₂), with highly variable amounts of FeO^{tot} (4.5–41.0 wt.%), BaO (0.1–34.5 wt.%) and Al₂O₃ (5.2–8.7 wt.%), and with a strong negative correlation between FeO^{tot} and BaO ($R^2 = -0.84$) (Figure 3). Type A slags are iron-rich and Type B slags are Ba-rich. Another difference between the types is in a slight enrichment of Type A samples with Al₂O₃ and K₂O (more prominent in Site 2 samples). The Type A samples have, on average, lower CaO content (3.1 wt.% of CaO) compared with the latter (7.7 wt.% of CaO). The Type A samples from Site 1 also exhibit slightly elevated MnO (1.1–5.9 wt.%) as well as ZnO (up to 6.7 wt.%) contents. The sulphur contents are on average higher for the Type A (1.0 wt.% of S^{tot}) compared with the Type B samples (0.6 wt.% of S^{tot}). It is also worth mentioning that the highest yet uniform values are linked to the Site 2 (Type A) slags (1.2–1.4 wt.% of S^{tot}). The content of P₂O₅ is relatively low (average 0.6 wt.% for Type A and 0.5 wt.% for Type B), but common for the given material; the only exceptions are samples ML25 (1.38 wt.% of P₂O₅) and ML26 (1.43 wt.% of P₂O₅). The As and Sb contents reach up to 269 ppm and 122 ppm, respectively. There are significantly

lower PbO contents in the Ba-rich slags (as low as 0.06 wt.%) with the exception of the ML24 (3.7 wt.%), ML25 (3.7 wt.%), ML26 (4.5 wt.%), and PL5 (5.7 wt.%) samples. The ML24 sample has the highest Ag content (331 ppm), whereas on average, there is 69 ppm of Ag in Type A and 79 ppm of Ag in Type B slags. Copper content varies among sites rather than between the slag types. Samples from the localities covering SHD area (Sites 2–4) have, after removal of minimum and maximum values, 463–974 ppm of Cu, whereas the copper content in the slags from the Site 1 is mostly higher and shows greater variance (740–2550 ppm). Similar trend is also observable for zinc contents (see Figure 3). The Cd content is low, with only one sample exceeding 10 ppm (PL5 with 40 ppm of Cd). What is particularly interesting is the perfect positive correlation between Sr and BaO ($R^2 = 1.00$).

Table 1. Bulk chemical composition of selected samples from studied localities in the JOD. *—ppb, Av—average, SG—specific gravity, b.d.—below the limit of detection, v.i.—viscosity index (calculated according to [1]), v.i.mod—viscosity index taking into account high PbO and ZnO contents (calculated according to [8]), liquidus—calculated by MELTS software [39].

Sample	PL5	PL7	PL8	PL15	ML2	ML7	ML24	ML26	JS4	JS6	JS9	CP1	CP4	CP7	Av	Min	Max	Av	Min	Max
Site	1	1	1	1	2	2	2	2	3	3	3	4	4	4	<i>n</i> = 19			<i>n</i> = 18		
Type	B	A	A	A	A	A	B	B	B	B	B	B	B	B	A	A	A	B	B	B
P ₂ O ₅ wt. %	0.67	0.94	0.95	0.55	0.53	0.59	0.44	1.43	0.41	0.43	0.32	0.39	0.39	0.36	0.60	0.37	0.99	0.51	0.30	1.43
SiO ₂	41.55	45.76	42.83	43.34	44.43	44.95	38.52	42.34	42.20	44.56	59.38	56.97	49.63	55.90	44.58	38.33	53.56	48.31	38.52	59.38
TiO ₂	1.00	0.42	0.27	0.42	0.38	0.38	0.97	0.94	0.54	0.55	0.39	0.24	0.65	0.33	0.37	0.27	0.45	0.57	0.24	1.00
Al ₂ O ₃	5.91	8.68	6.07	7.10	6.76	6.84	6.35	6.46	6.21	6.20	6.06	5.53	6.25	5.85	6.98	5.57	8.68	6.08	5.24	6.76
BaO	23.20	0.42	1.32	2.05	1.04	1.16	34.50	27.69	22.60	19.20	11.61	8.16	19.54	5.44	0.94	0.08	2.10	18.92	5.44	34.50
CaO	7.68	4.15	3.07	3.90	2.74	2.63	6.51	6.20	10.46	10.59	5.71	4.77	7.16	4.85	3.09	2.49	4.15	7.77	4.57	10.59
FeO ^{tot}	8.80	22.62	31.29	24.97	38.66	37.29	4.51	4.89	11.19	10.96	10.91	16.67	11.26	20.49	31.93	21.85	41.01	11.07	4.51	20.49
MgO	1.49	1.40	1.39	1.74	1.10	1.11	1.42	1.28	1.41	1.36	0.97	0.79	1.24	1.02	1.16	0.84	1.81	1.24	0.79	1.68
MnO	0.34	3.15	5.87	2.36	0.30	0.37	0.13	0.20	0.34	0.35	0.27	0.63	0.32	0.59	1.76	0.27	5.87	0.34	0.13	0.63
PbO	5.74	5.57	3.25	3.91	0.91	0.92	3.65	4.47	0.54	0.93	0.20	0.23	0.72	0.23	2.77	0.81	5.77	1.24	0.06	5.74
ZnO	1.53	3.72	2.25	5.68	1.10	1.11	0.75	0.19	1.29	1.24	1.17	0.72	0.95	0.41	2.59	0.64	6.65	0.83	0.18	1.68
K ₂ O	2.26	3.32	2.09	2.79	2.36	2.38	1.85	2.56	2.02	2.11	1.97	2.22	2.08	2.33	2.64	2.09	3.48	2.10	1.63	2.71
Na ₂ O	0.52	0.80	0.45	0.95	0.54	0.53	0.46	0.66	0.69	0.52	0.44	0.38	0.59	0.45	0.60	0.43	1.03	0.53	0.38	0.71
S ^{tot}	0.31	0.73	1.05	0.79	1.21	1.34	0.88	0.17	0.54	0.49	0.65	0.80	0.45	0.65	1.02	0.62	1.36	0.53	0.17	0.88
Total	101.00	101.68	102.15	100.54	102.06	101.59	100.94	99.49	100.44	99.49	100.06	98.50	101.22	98.89	101.04	98.30	102.15	100.04	98.50	101.34
Ag ppm	38	32	112	23	77	78	331	91	77	93	11	51	28	64	69	3	144	79	2	331
As	39	80	86	49	7	8	23	24	b.d.	9	46	18	70	14	47	3	269	28	6	71
Au *	b.d.	20	40	b.d.	34	41	5	5	b.d.	5	0	4	b.d.	9	39	8	86	5	0	9
Cd	39.5	1.5	2.1	2.2	0.4	0.8	0.3	b.d.	b.d.	1.6	4.9	4.0	9.3	1.1	1.4	b.d.	2.2	5.7	0.3	39.5
Co	60	26	22	31	12	16	4	10	82	26	137	36	82	28	27	10	53	60	4	137
Cr	90	120	80	b.d.	60	60	80	120	b.d.	60	50	60	90	70	87	42	147	79	40	120
Cu	740	2470	1120	1530	684	706	138	717	923	910	1860	763	974	961	1220	652	2550	833	138	1860
Ni	11	107	37	28	10	32	5	15	b.d.	75	84	9	84	96	25	9	107	38	5	96
Sb	2	122	21	38	21	19	71	103	36	55	9	15	2	13	29	8	122	31	2	103
Sn	7	4	17	b.d.	2	2	b.d.	19	b.d.	b.d.	6	5	5	2	6	b.d.	17	10	1	31
Sr	4470	253	344	459	249	266	6680	5550	4310	3820	2280	1516	3570	1090	260	158	529	3520	1090	6680

v.i.mod	1.09	0.83	1.04	0.96	0.95	0.92	1.20	0.99	1.04	0.93	0.51	0.55	0.78	0.58	0.93	0.64	1.15	0.84	0.51	1.20
v.i.	0.93	0.66	0.93	0.77	0.91	0.88	1.10	0.89	1.01	0.89	0.49	0.54	0.75	0.57	0.83	0.53	0.99	0.80	0.49	1.13
SG g/cm ³	3.47	3.15	3.38	3.44	3.31	3.28	3.24	3.04	3.27	3.13	2.99	3.02	2.86	3.04	3.27	2.77	3.53	3.07	1.83	3.47
liquidus °C	1122	1164	1188	1162	1183	1182	1121	1087	1114	1139	1081	1093	1093	1105	1178	1147	1260	1110	1075	1153

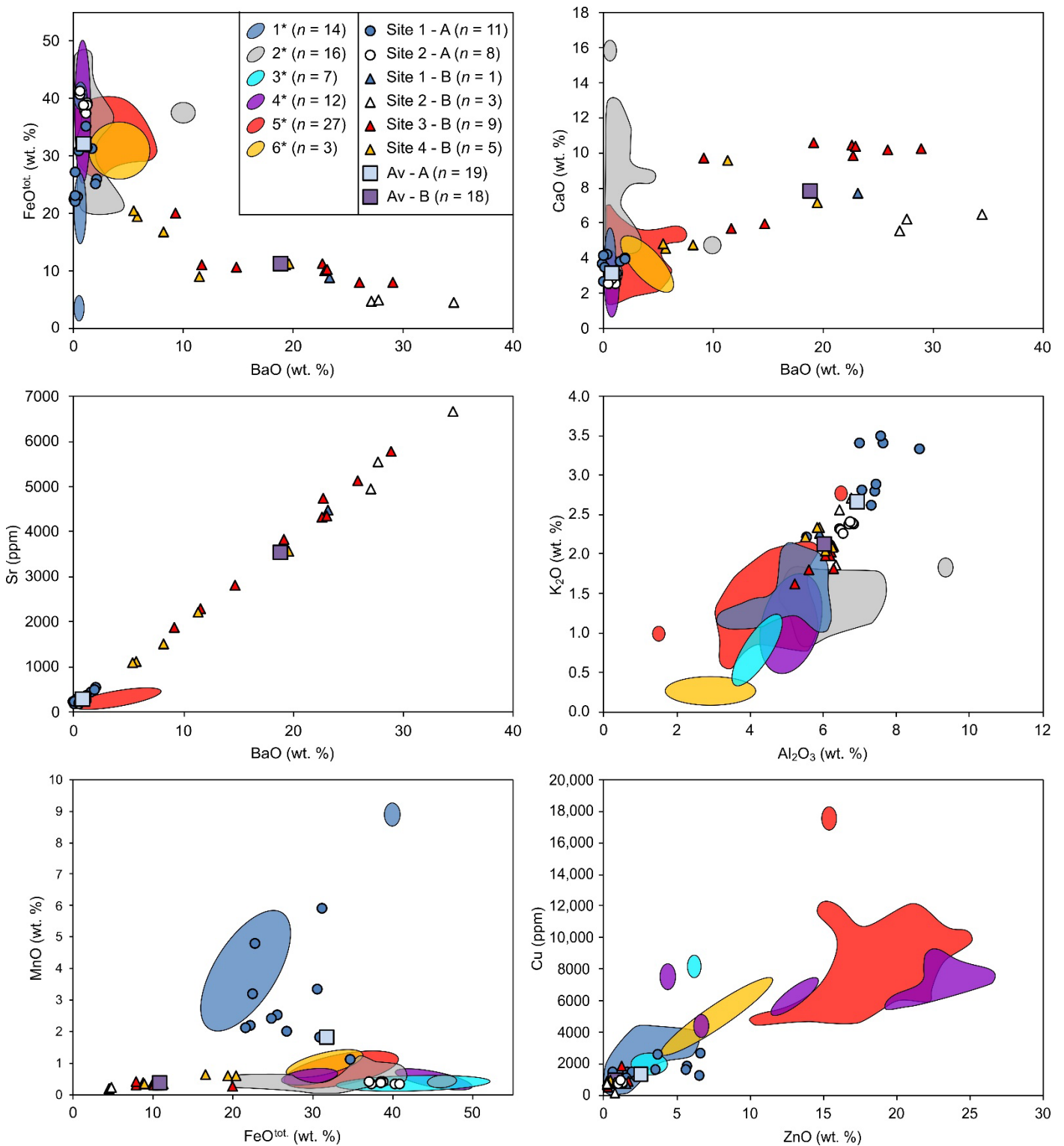


Figure 3. Selected bivariate plots highlighting the differences in bulk chemical composition of the Type A and B slags from individual sites. Av—average, comparative data: 1*—Příbram (Czech Republic; [8]), 2*—Wiesloch (Germany; [9]), 3*—Kutná Hora (Czech Republic; [6]), 4*—Harz (Germany; [40]), 5*—Harz (Germany; [41]), 6*—Harz (Germany; [42]).

5.2. Slag Mineralogy and Crystal Chemistry

Identified phase assemblages are listed in Table 2. The biggest difference is between assemblage II and the rest, caused by the exceptional amount of glass. The XRD data show

that the crystalline phases in assemblage II comprise between 0.5–7.9%, whereas for the assemblages I and III they are over 52.0%. The assemblage II with all listed phases is limited to a single sample (J55), whereas the association of glass, accessory feldspar, quartz and the inclusions of metals and matte are dominant. Assemblage I and III are much alike in terms of diverse olivine morphology; however, they differ in presence/absence of feldspar and pyroxene. All crystalline phases, except for olivine group, are only accessory. Typical phases of sulfidic inclusions are pyrrhotite, rudashevskyite, and less galena. Interstitials are filled by the bornite-like phase (Cu-Fe-S). A Fe-Cu-Ba-S phase has the same role in some of the Type B samples. Breithauptite, dyscrasite, and FeAs phase are rare. Native metals are represented by copper, iron, silver, and lead, which is the most abundant. Another constituent of the samples is partially melted quartz.

Table 2. Phase assemblages identified in studied slags by combination of optical microscopy, electron microprobe, and XRD.

Assemblage	Phases	Slag Type	Site
I	Gl + Ol	A	1, 2
II	Gl + Fld ± Wo ± Px ± Mel	B	1, 2, 3, 4
III	Gl + Ol + Fld ± Px	A	1

Olivine is a typical crystalline phase of assemblages I and III. Its shape may range from euhedral and hopper-like crystals through skeletal laths to feather-like aggregates within a single sample. The overall dimensions of olivine crystals are in range of 10–100 μm , but in some cases (Site 1) the laths reach up to a few mm. In some samples, there are clearly distinguishable two adjacent generations of olivine crystals, the first being skeletal laths tenths of μm in size and the second in the form of minute laths reflecting rapid crystallization from interstitial glass (Figure 4e). The chemical complexity of olivine composition is observable among sites, but also on the level of a single sample (Table 3). Interestingly, the main variation within a sample is caused by $\text{Mg}^{2+} \leftrightarrow \text{Fe}^{2+}$ substitution, whereas the contents of other divalent cations (Ca, Mn, Zn) are usually rather stable. On the other hand, zonation of a single crystal is negligible. The composition of Site 1 olivine varies from fayalite-dominated phase (65–81 mol.% of Fa) to fayalite enriched by forsterite (0–22 mol.% of Fo) and tephroite (4–13 mol.% of Tep). Olivine can comprise up to 18 mol.% of willemite (Zn_2SiO_4) into its structure [9] (and references there in), but this limit is not reached because the detected maximum for Site 1 is 14 mol.% of Wi. The CaO contents are very low; therefore, the DCS (Ca_2SiO_4) molecule is almost negligible (not exceeding 4 mol.% of DCS).

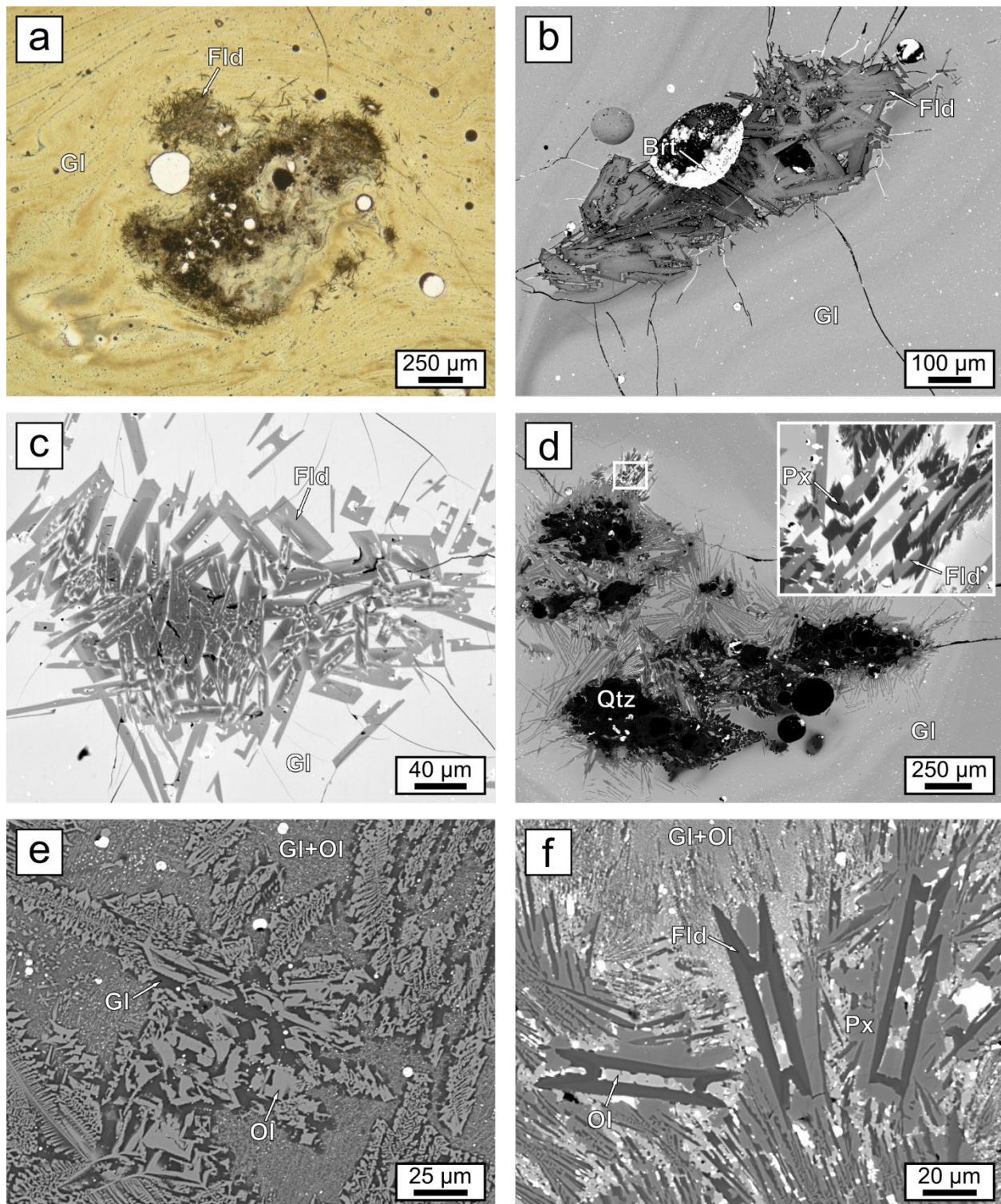


Figure 4. Images in transmitted parallel polarized light (a) and BSE (the rest) of A (a–d) and B (the rest) Type slags from the studied localities. (a) aggregate of feldspars (Fld) surrounded by yellowish-green glass with fluidal texture (Gl) (CP4); (b) zonation of feldspars and surrounding glass, secondary baryte (Brt) inside pore (ML25); (c) distinctive zonation of feldspars on the level of a whole aggregate (ML24); (d) long laths of feldspar and short columns of pyroxene (Px) crystallized around quartz relicts (Qtz) (JS6); (e) two generations of olivine (PL8); (f) slightly zoned feldspar laths surrounded by pyroxene and olivine (PL15). Po—pyrrhotite, Gl—glass.

The olivine from Site 2 is quasi-pure fayalite (87–96 mol.%), marginally substituted on average by 4 mol.% of forsterite. The contribution of other endmembers is low, not

exceeding 3 mol.%. The main difference in olivine composition between given localities narrows to higher contents of ZnO and MnO for Site 1, as can be seen from the ternary plots (Figure 5a,b). Olivines from Site 1 are also on average richer in MgO. The presence of up to 1.78 wt.% of Al₂O₃, 0.54 wt.% of BaO, 0.46 wt.% of PbO and 0.67 wt.% of K₂O in point analyses could be addressed by sub-microscopic inclusions of glass [43].

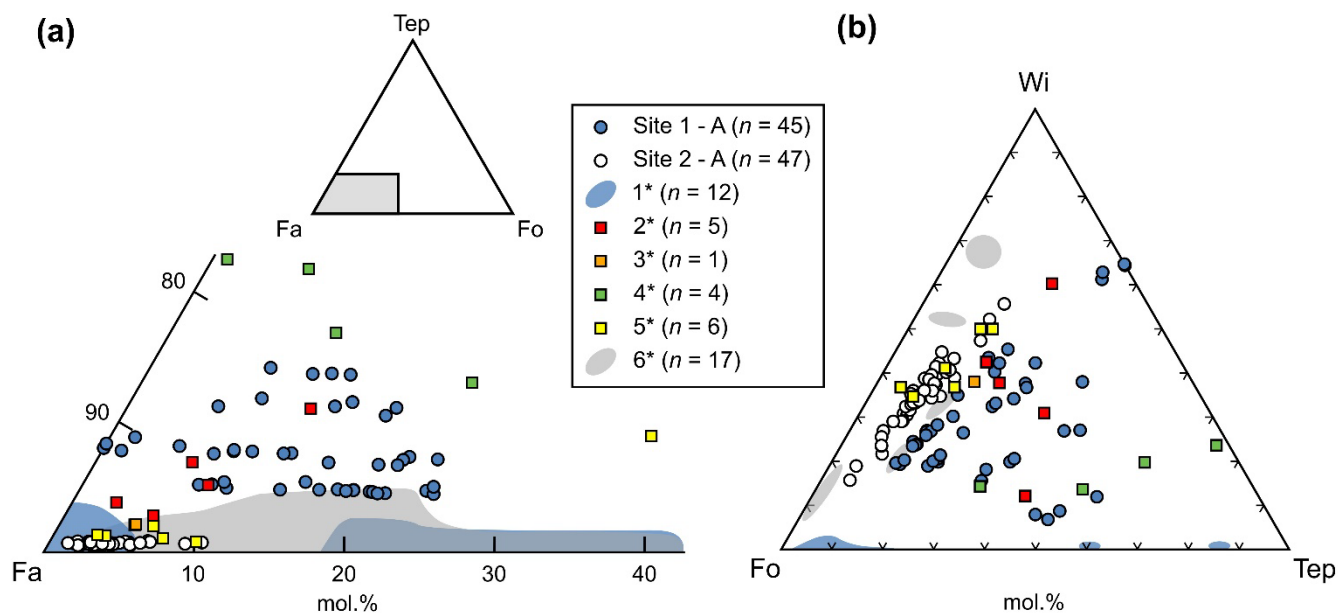


Figure 5. Composition of olivine projected into the Tep-Fa-Fo (a) and Wi-Fo-Tep ternary plots (b). Comparative data: 1*—Lower Silesia (Poland; [10]), 2*—Příbram (Czech Republic; [44]), 3*—Kutná Hora (Czech Republic; [6]), 4*—Příbram (Czech Republic; [8]), 5*—Capattoli Valley (Italy; [4]), 6*—Wiesloch (Germany; [9]).

Pyroxene was identified only in Type A slags from Site 1 (assemblage III) and Type B slags from Site 3. Pyroxene forms euhedral to subhedral short columns and almost square or rhombic cross sections in Type B slags. The size of the largest crystals does not exceed the first tenths of μm . The chemical composition of pyroxenes splits into two groups (Table 3). The first group is rather uniform ($\text{Wo}_{50-51}\text{En}_{31-35}\text{Fs}_{15-19}$) and plots in the Wo-En-Fs ternary diagram [45] on the very border of the diopside and Wo-rich pyroxene field (Figure 6a). The second group corresponds to Wo-rich pyroxenes with distinctive trend toward the Wo peak ($\text{Wo}_{76-90}\text{En}_{4-10}\text{Fs}_{6-15}$). The contents of other oxides do not exceed 2 wt.% (e.g., 0.3–0.6 wt.% of MnO, 0.4–0.7 wt.% of ZnO and 0.9–1.6 wt.% of Al₂O₃). Pyroxenes from Site 1 form subhedral to anhedral crystals and short columns a few tenths of μm in length, which are usually spatially bound to feldspar. Their composition is characterized by the variation of CaO (2.2–27.7 wt.%) and FeO (13.6–37.0 wt.%) contents (Wo-Fs end members). Most of the analyses group in the Wo-En-Fs ternary plot [45] within the field of hedenbergite with some overlaps into the field of Wo-rich pyroxene and augite. The rest falls in the field of pigeonite close to the Fs peak (Figure 6a). The complete composition of presented groups of pyroxenes from Type A slags could be expressed as $\text{Wo}_{31-44}\text{En}_{4-10}\text{Fs}_{31-44}\text{Knt}_{2-12}\text{Pdu}_{6-14}\text{Tsch}_{0-5}$ and $\text{Wo}_{2-8}\text{En}_{8-24}\text{Fs}_{54-66}\text{Knt}_{7-11}\text{Pdu}_{6-13}\text{Tsch}_{2-4}$, once the elevated contents of MnO (1.1–6.7 wt.%) and ZnO (1.8–4.5 wt.%) are projected in kanoite (theoretical formula $\text{Mn}_2\text{Si}_2\text{O}_6$ was considered for calculation) and petedunnite ($\text{CaZnSi}_2\text{O}_6$) components.

Table 3. Representative compositions of olivine, pyroxene, and wollastonite. The apfu values are calculated based on 4 oxygens for olivine, 6 oxygens for pyroxene, and 9 oxygens for wollastonite. b.d.—below the limit of detection.

Phase	O1	O1	O1	O1	O1	O1	O1	Px	Px	Px	Px	Wo	Wo
An. No.	18/1.	17/1.	56/1.	1/1.	99/1.	82/1.	114/1.	67/1.	46	74/1.	4	28/1.	32/1.
Sample	ML1	ML1	PL1	PL1	PL2	PL7	PL8	PL1	PL15	PL7	JS5	JS5	JS5
Site	2	2	1	1	1	1	1	1	1	1	3	3	3
Type	A	A	A	A	A	A	A	A	A	A	B	B	B
P ₂ O ₅ wt. %	0.50	b.d.	b.d.	b.d.	b.d.	b.d.	b.d.	0.33	b.d.	b.d.	b.d.	b.d.	b.d.
SiO ₂	29.57	30.80	30.94	31.64	30.71	30.19	31.11	45.65	44.92	46.80	51.36	51.31	51.92
TiO ₂	b.d.	b.d.	b.d.	b.d.	b.d.	b.d.	b.d.	1.23	0.27	b.d.	0.52	b.d.	0.21
Al ₂ O ₃	b.d.	b.d.	b.d.	b.d.	b.d.	b.d.	b.d.	3.17	3.13	0.43	1.03	b.d.	0.62
BaO	b.d.	b.d.	b.d.	b.d.	b.d.	b.d.	b.d.	b.d.	b.d.	b.d.	b.d.	b.d.	0.39
CaO	0.40	0.41	0.52	0.45	0.46	1.30	0.39	19.28	6.38	16.78	24.01	46.97	45.12
FeO	63.31	62.85	51.41	49.78	49.16	47.24	51.43	22.43	33.67	23.29	9.49	0.59	0.77
MgO	2.54	2.45	6.83	9.15	7.75	6.70	5.40	2.66	2.63	1.24	11.74	b.d.	b.d.
MnO	0.52	0.56	3.14	3.45	4.75	7.29	9.52	1.25	3.75	6.19	0.34	b.d.	0.23
PbO	b.d.	b.d.	b.d.	b.d.	b.d.	0.21	b.d.	b.d.	b.d.	0.37	b.d.	b.d.	b.d.
ZnO	1.76	1.55	6.33	5.72	5.47	4.86	1.88	2.98	4.00	2.90	0.59	b.d.	b.d.
K ₂ O	0.07	0.14	b.d.	b.d.	b.d.	b.d.	b.d.	0.09	b.d.	b.d.	b.d.	b.d.	b.d.
Sum	98.67	98.76	99.17	100.20	98.30	97.79	99.73	99.07	98.75	98.00	99.08	98.87	99.26
P ⁵⁺ apfu	0.000	0.000	0.000	0.000	0.000	0.000	0.000	0.007	0.000	0.000	0.000	0.000	0.000
Si ⁴⁺	0.996	1.028	1.007	1.003	1.002	0.998	1.010	1.877	1.914	1.989	1.960	3.010	3.023
Ti ⁴⁺	0.000	0.000	0.000	0.000	0.000	0.000	0.000	0.038	0.009	0.000	0.015	0.000	0.009
Al ³⁺	0.000	0.000	0.000	0.000	0.000	0.000	0.000	0.154	0.157	0.022	0.046	0.000	0.043
Ba ²⁺	0.000	0.000	0.000	0.000	0.000	0.000	0.000	0.000	0.000	0.000	0.000	0.000	0.009
Ca ²⁺	0.014	0.015	0.018	0.015	0.016	0.046	0.014	0.850	0.291	0.764	0.982	2.952	2.815
Fe ²⁺	1.784	1.754	1.399	1.320	1.341	1.306	1.397	0.771	1.200	0.828	0.303	0.029	0.037
Mg ²⁺	0.128	0.122	0.331	0.432	0.377	0.330	0.261	0.163	0.167	0.079	0.668	0.000	0.000
Mn ²⁺	0.015	0.016	0.087	0.093	0.131	0.204	0.262	0.044	0.136	0.223	0.011	0.000	0.011
Pb ²⁺	0.000	0.000	0.000	0.000	0.000	0.000	0.000	0.000	0.000	0.004	0.000	0.000	0.000
Zn ²⁺	0.044	0.038	0.152	0.134	0.132	0.119	0.045	0.090	0.126	0.091	0.017	0.000	0.000
K ⁺	0.000	0.000	0.000	0.000	0.000	0.000	0.000	0.005	0.000	0.000	0.000	0.000	0.000
Catsum	2.981	2.972	2.993	2.997	2.998	3.002	2.990	3.999	3.999	4.000	4.002	5.990	5.947

Wollastonite is exclusive in Type B slags (assemblage II), where is present in the form of euhedral to subhedral short columns and laths. The overall small size of crystals (< 10 µm) does not allow to determine chemical zonation. The wollastonite is relatively pure (2.82–2.95 apfu Ca) with only minor contents of FeO (0.59–0.77 wt.%), Al₂O₃ (0.62 wt.%), BaO (0.39 wt.%), MnO (0.23 wt.%) and TiO₂ (0.21 wt.%), which could be partially addressed by the small size of the analysed crystals.

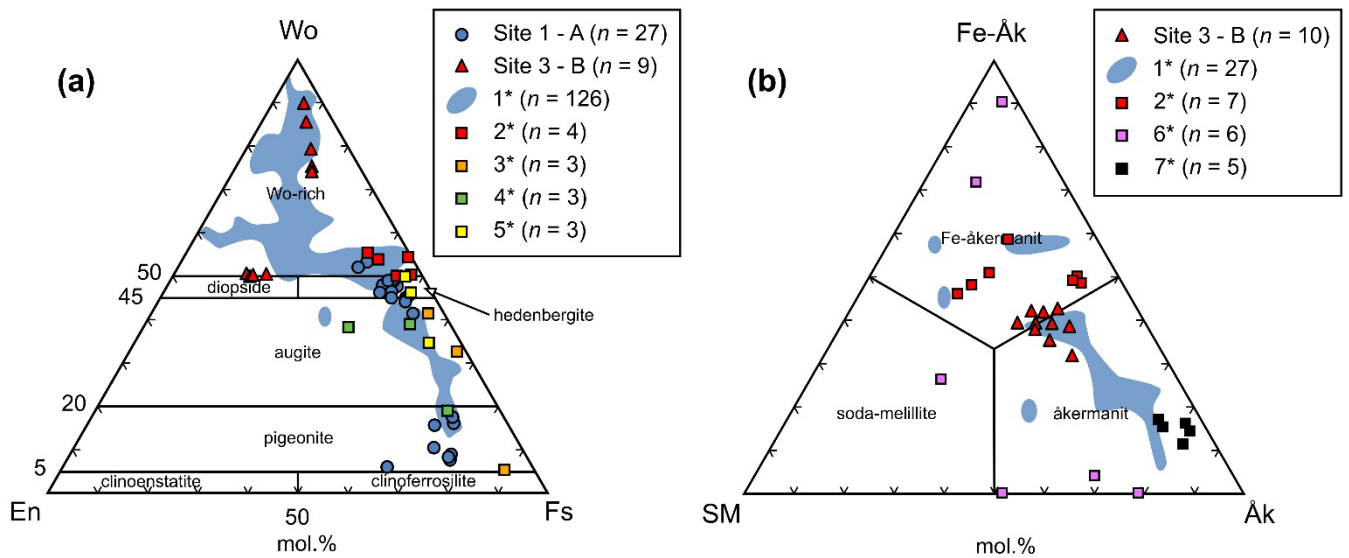


Figure 6. Compositions of pyroxene projected in the ternary system Wo-En-Fs (a) (according to [45]) and melilites plotted in FeÅk-SM-Åk ternary diagram (b). SM—soda melilite, comparative data: 1*—Lower Silesia (Poland; [10]), 2*—Příbram (Czech Republic; [44]), 3*—Kutná Hora (Czech Republic; [6]), 4*—Příbram (Czech Republic; [8]), 5*—Massa Maritima (Italy; [5]), 6*—Prague (Czech Republic; [46]), 7*—Silesian-Cracovian region (Poland; [11]).

Melilite is a very rare phase restricted to Type B slags and identified only in a single sample from Site 3 (JS5). The melilite is represented by euhedral to subhedral tabular crystals tenths of μm long, which form H-shaped aggregates in omnipresent glass. The chemical variability of studied melilites is apparent from Table 4. The composition is dominated by åkermanite (30–42 mol.%) and ferro-åkermanite (27–35 mol.%) followed by soda melilite (13–22 mol.%). Relatively high contents of ZnO (2.4–4.7wt.%) are projected in 10–17 mol.% of hardystonite. The gehlenite molecule is rather negligible (1–8 mol.%). The composition of melilites projects in the FeÅk-SM-Åk ternary plot around the border between ferro-åkermanite and the åkermanite field (Figure 6b). The unusual bulk composition of the JS5 sample is responsible for the partial substitution of Ca^{2+} by Ba^{2+} (0.03–0.07 apfu Ba).

Table 4. Representative compositions of melilite and feldspar. The apfu values were calculated on the basis of 7 oxygens for melilite and 8 oxygens for feldspar. Av—average, b.d.—below the limit of detection, - not analysed.

Phase	Mel	Mel	Mel	Fld	Fld	Fld	Fld	Fld	Fld	Fld	Fld	Fld	Fld
An. No.	35/1.	30/1.	29/1.	65/1.	$n = 19$			122/1.	139/1.	164/1.	$n = 28$		
Sample	JS5	JS5	JS5	PL1	Av	Min	Max	JS9	CP5	ML26	Av	Min	Max
Site	3	3	3	1	1	1	1	3	4	2	1–4	1–4	1–4
Type	B	B	B	A	A	A	A	B	B	B	B	B	B
P_2O_5 wt.%	b.d.	b.d.	0.35	b.d.	b.d.	b.d.	b.d.	b.d.	b.d.	0.16	0.18	0.16	0.19
SiO_2	41.39	41.00	40.01	52.67	56.35	51.05	61.63	47.82	41.99	45.02	43.59	32.87	52.43
Al_2O_3	4.49	3.89	4.64	20.72	21.31	18.97	26.82	16.25	24.77	17.69	21.15	16.25	24.77
Fe_2O_3	-	-	-	0.77	1.20	0.51	1.84	4.77	0.37	1.72	1.35	0.27	4.77
BaO	2.29	1.64	3.35	14.13	6.33	0.55	14.13	22.38	27.11	26.45	26.08	14.88	38.82
CaO	34.96	35.07	34.47	0.36	3.12	0.12	12.08	1.14	1.16	0.95	0.58	0.07	2.53
FeO	6.27	7.54	6.62	-	-	-	-	-	-	-	-	-	-
MgO	4.77	4.23	4.79	b.d.	b.d.	b.d.	b.d.	0.46	b.d.	0.86	0.47	0.13	1.00
MnO	0.53	b.d.	0.46	b.d.	0.20	0.16	0.30	b.d.	b.d.	b.d.	0.17	0.16	0.19
PbO	b.d.	b.d.	b.d.	0.53	1.29	0.35	3.72	b.d.	b.d.	0.40	0.63	0.21	1.71
SrO	b.d.	b.d.	b.d.	0.16	0.18	0.15	0.25	0.19	0.49	b.d.	0.23	0.14	0.49

ZnO	2.74	4.65	2.75	0.31	0.36	0.16	0.75	1.04	b.d.	0.15	0.43	0.15	1.04
K ₂ O	0.65	0.39	0.54	9.84	8.52	1.55	12.05	5.96	3.82	5.26	4.78	0.71	7.25
Na ₂ O	1.39	1.63	0.94	0.47	1.62	0.42	5.77	0.46	0.55	0.35	0.52	0.21	1.49
Sum	99.48	100.04	98.92	99.88	99.28	97.62	101.12	99.99	100.22	98.84	98.81	97.56	100.41
P ⁵⁺ apfu	0.000	0.000	0.009	0.000	0.000	0.000	0.008	0.000	0.000	0.000	0.001	0.000	0.009
Si ⁴⁺	1.989	1.980	1.954	2.702	2.734	2.424	2.936	2.628	2.344	2.502	2.463	2.093	2.670
Al ³⁺	0.254	0.221	0.267	1.253	1.217	1.079	1.497	1.053	1.630	1.379	1.417	1.053	1.796
Fe ³⁺	-	-	-	0.030	0.044	0.017	0.067	0.197	0.015	0.044	0.057	0.011	0.197
Ba ²⁺	0.043	0.031	0.064	0.284	0.110	0.000	0.284	0.482	0.593	0.593	0.585	0.297	0.969
Ca ²⁺	1.800	1.814	1.804	0.020	0.158	0.006	0.622	0.067	0.069	0.004	0.034	0.004	0.138
Fe ²⁺	0.252	0.304	0.270	-	-	-	-	-	-	-	-	-	-
Mg ²⁺	0.342	0.304	0.349	0.000	0.000	0.000	0.000	0.038	0.000	0.043	0.024	0.000	0.085
Mn ²⁺	0.022	0.000	0.019	0.000	0.003	0.000	0.012	0.000	0.000	0.000	0.001	0.000	0.009
Pb ²⁺	0.000	0.000	0.000	0.007	0.016	0.000	0.049	0.000	0.000	0.003	0.002	0.000	0.026
Sr ²⁺	b.d.	b.d.	b.d.	0.005	0.002	0.000	0.007	0.006	0.016	0.006	0.007	0.000	0.016
Zn ²⁺	0.097	0.166	0.099	0.012	0.009	0.000	0.026	0.042	0.000	0.000	0.009	0.000	0.042
K ⁺	0.040	0.024	0.034	0.644	0.533	0.090	0.732	0.418	0.272	0.383	0.343	0.058	0.499
Na ⁺	0.130	0.153	0.089	0.047	0.149	0.041	0.509	0.049	0.060	0.044	0.051	0.000	0.152
Catsum	4.969	4.998	4.959	5.002	4.976	4.890	5.019	4.980	4.999	5.000	4.996	4.885	5.025

The morphology and chemical composition of **feldspar** is determined by the slag type. Feldspar is the main and sometimes sole newly formed crystalline phase amongst silicates in Type B slags; thus, it is represented by euhedral laths (hundreds of μm long), tabular crystals (up to 200 μm long), and complex aggregates. A common phenomenon is grouping of laths around quartz grains (Figure 4d). A strong chemical zonation is typical (Figure 4c), which is mainly caused by the heterovalent substitution of $\text{Al}^{3+} + \text{Ba}^{2+} \leftrightarrow \text{Si}^{4+} + \text{K}^+$. The cores of crystals are usually enriched in K_2O (up to 12.5 wt.%) with celsian endmember ($\text{BaAl}_2\text{Si}_2\text{O}_8$) gradually increasing toward the rim. The highest recorded BaO content in a rim is 38.8 wt.%, which corresponds to 93 mol.% of Cls. Reverse zonation, with Ba-rich cores, is observable only rarely (Figure 4b). The presence of barium is also linked to the relative enrichment in Sr (up to 0.5 hm.%, equivalent to 2 mol.% of slawsonite). Other constituents are anorthite (0–16 mol.%), albite (0–17 mol.%), and lead feldspar (0–3 mol.%). Some feldspars have elevated Fe_2O_3 (up to 4.8 wt.%) contents.

Feldspars from the assemblage III (slag Type A) tend to form complex intergrowths with surrounding phases. Typical are short to long subhedral laths to anhedral grains, reaching up to 100 μm in length. The chemical zonation is usually less prominent. Common is the dominance of orthoclase (average 55 mol.%); however, albite and anorthite end members contribute significantly to the overall composition (up to 58 and 57 mol.%, respectively), followed by minor amount of lead feldspar (up to 5 mol.%), and slawsonite (up to 1 mol.%). Surprisingly, the feldspar can concentrate up to 14.1 wt.% of BaO despite the generally low barium bulk contents (on average 0.9 wt.% of BaO for Type A slags).

Glass is a common component of all samples and its colour in transmitted light is strongly dependent on the slag type rather than on assemblage and vary from opaque (Type A) to yellowish-green, with a visible fluidal texture highlighted by colour change and minute opaque inclusions (Type B) (Figure 4a). A few tenths of μm thick layer of translucent greenish or/and brownish glass are often developed around quartz grains even in opaque domains. The chemical composition of glass is usually a rough reflection of respective bulk composition. In fact, a series of point analyses could serve as a legit substitution of bulk data in a glassy homogenous slag with only minor inclusions of quartz and metallic compounds, as seen on the example of sample JS1 in Table 5. The glasses from the Type A slags are chiefly composed of SiO_2 (average 44.6 wt.% in slags from Site 1 and 52.1 wt.% in slags from Site 2), FeO (22.9 wt.% and 21.5 wt.%), Al_2O_3 (8.2 wt.% and 10.5 wt.%) and CaO (6.4 wt.% and 5.0 wt.%). SO_3 (average 1.1 wt.% in slags from

Site 1 and 1.3 wt.% in slags from Site 2) and P₂O₅ (1.0 wt.% and 1.1 wt.%) contents are relatively high. The main difference in composition of the Type A glass between localities is in the higher contents of MnO (average 1.9 wt.% in slags from Site 1 and 0.26 wt.% in slags from Site 2), PbO (5.6 wt.% and 1.2 wt.%) and ZnO (3.4 wt.% and 1.2 wt.%) for the slags from Site 1.

Table 5. Chemical composition of glass from JOD slags. Averages calculated from WDS and EDS. Av—average, SD—standard deviation, Rep.—representative analysis, bulk—bulk chemical composition, b.d.—below the limit of detection, - not calculated.

Sample	n = 70			n = 86		n = 7		n = 18		n = 61		n = 6	
	Av	SD	Rep.	Av	SD	Av	SD	Av	SD	Av	SD	Av	Bulk
Site	1	1	1	2	2	2	2	4	4	3	3	3	3
Type	A	A	B	A	A	B	B	B	B	B	B	B	B
SO ₃ wt.%	1.22	0.79	0.77	1.26	0.59	0.55	0.38	0.65	0.38	0.88	0.32	0.55	0.53
P ₂ O ₅	0.95	0.42	0.07	1.11	0.42	1.39	0.34	0.57	0.43	0.34	0.11	0.24	0.37
SiO ₂	44.58	5.91	40.79	52.07	6.86	41.64	3.25	50.67	4.81	46.24	6.31	43.42	44.05
TiO ₂	0.64	0.37	b.d.	0.71	0.39	1.16	0.21	0.43	0.15	0.61	0.18	b.d.	0.48
Al ₂ O ₃	8.15	2.19	7.15	10.52	1.93	6.19	0.87	7.96	2.81	6.12	1.73	5.78	5.61
BaO	1.66	1.33	35.01	2.23	0.85	32.42	4.18	11.52	2.75	20.26	6.98	26.26	25.90
CaO	6.40	3.29	5.90	4.96	1.81	6.42	0.93	7.91	2.67	9.41	2.77	10.42	10.17
FeO	22.92	12.72	5.54	21.53	8.03	4.25	0.29	13.69	6.06	10.54	4.61	7.50	7.93
MgO	0.78	0.50	1.24	0.43	0.40	1.12	0.17	1.31	0.37	1.00	0.34	1.10	1.40
MnO	1.92	0.96	b.d.	0.26	0.05	0.31	0.00	0.67	0.43	0.23	0.16	0.34	0.28
PbO	5.59	3.59	0.57	1.18	0.45	2.16	0.54	0.45	0.43	0.17	0.34	0.14	0.25
SrO	b.d.	-	b.d.	0.05	0.07	0.44	0.11	b.d.	-	0.05	0.12	b.d.	0.61
ZnO	3.44	1.72	0.78	1.19	0.37	0.44	0.35	1.23	0.72	1.58	1.54	0.94	0.93
K ₂ O	2.21	0.92	1.61	3.10	0.84	2.42	0.73	2.43	0.62	2.02	0.86	1.75	1.80
Na ₂ O	0.81	0.29	0.43	0.77	0.18	0.60	0.12	0.69	0.28	0.52	0.20	0.54	0.42
Sum	99.41	1.27	99.87	100.22	1.09	98.82	0.86	98.67	1.20	99.15	0.73	99.53	100.12
v.i.	0.74	0.40	1.04	0.55	0.20	1.00	0.19	0.66	0.18	0.87	0.20	0.97	0.99
v.i.mod	0.91	0.39	1.07	0.59	0.20	1.05	0.17	0.69	0.18	0.90	0.21	1.00	0.96

The glass composition of Site 4 slags represents “bridge” between Type A and Type B samples. The reason is in average high SiO₂ (50.67 wt.%), FeO (13.7 wt.%), and Al₂O₃ (8.0 wt.%) contents compared to the glass of Type B slags and simultaneously an order of magnitude higher BaO (11.5 wt.%) content than in the glass from Type A slags. The contents of CaO (average 7.9 wt.%) and minor oxides are similar to the other Type B glasses.

The chemical composition of Type B glass from Sites 2 and 3 is dominated by SiO₂ (average 41.6 wt.% and 46.2 wt.%, respectively), BaO (32.4 wt.% and 20.3 wt.%), FeO (4.3 wt.% and 10.6 wt.%), CaO (6.4 wt.% and 9.4 wt.%), and Al₂O₃ (6.2 wt.% and 6.1 wt.%). Contents of P₂O₅ (average 1.4 wt.%) and PbO (2.4 wt.%) are slightly elevated for the Site 2 slags. The Type B glass from Site 1 is represented by a single analysis and its chemical composition is comparable to similar material from Site 2 and 3 (40.8 wt.% of SiO₂, 35.0 wt.% of BaO, 7.2 wt.% of Al₂O₃, 5.9 wt.% of CaO, and 5.5 wt.% of FeO).

The translucent rims along quartz grains are a result of their partial melting, therefore their composition is rich in Al₂O₃, SiO₂, and K₂O and depleted in FeO, CaO, and other minor oxides.

Secondary phases result from the dissolution/weathering of unstable phases such as sulphides and glass, which is more stable compared with the former, but represents a large volume of all samples. Sulphate phases occupy pores or voids associated with dissolution of metallic and/or sulphidic inclusions. In some cases, they even crystallize in

interstitial spaces among still-present sulphides (Figure 7a). The sulphates tend to form few tenths of μm long euhedral to subhedral tabular crystals. The chemical composition of analysed sulphates proves high miscibility in the $\text{BaSO}_4\text{-PbSO}_4$ system, which is also well documented by the strong zonation visible on BSE images (Figure 7b). The dominant endmember is baryte, in part of analyses strongly substituted by Pb (up to 0.23 apfu Pb) (Table 6). Other admixtures are represented chiefly by FeO (up to 3.1 wt.%), CuO (1.4 wt.%), CaO (up to 1.0 wt.%), and only rarely by SrO (up to 1.6 wt.%). Hydrous ferric oxides in both types of slags were not subjected to detailed study.

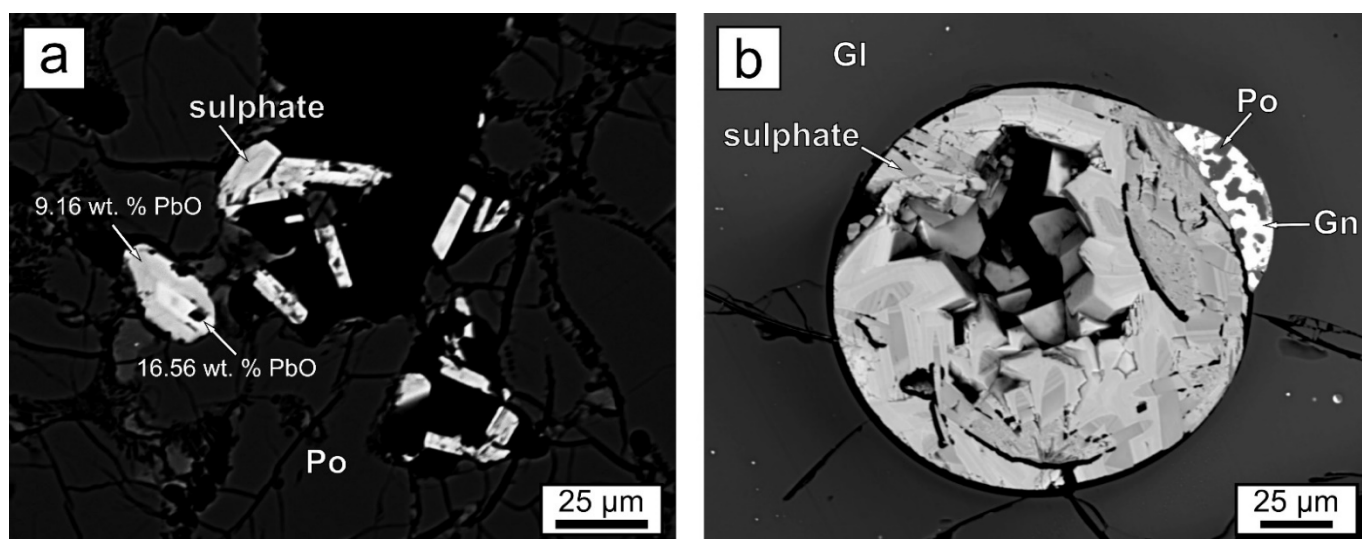


Figure 7. Examples of sulphates, sulphides, and metals in the slags. Photos in BSE. (a) zonal sulphates inside sulphidic inclusion (JS9); (b) sulphate as an infilling of pore bordering with galena (Gn) dominated by small sulphidic inclusion (PL5). Po—pyrrhotite, Gl—glass.

Table 6. Representative compositions of sulphates. The apfu values were calculated on the basis of 4 oxygens. b.d.—below the detection limit.

An. No.	36/1.	37/1.	40/1.	41/1.	22/1.	28/1.	6/1.	33/1.	42/1.	44/1.	45/1.	49/1.
Sample	JS9	JS9	JS9	JS9	CP5	CP5	CP5	CP5	CP10	CP10	CP10	CP10
Site	3	3	3	3	4	4	4	4	4	4	4	4
SO_3 wt. %	34.05	34.12	33.39	33.17	35.26	35.05	33.45	35.20	34.15	33.95	34.77	34.17
BaO	55.43	55.29	51.97	52.07	60.12	59.90	39.93	61.55	63.37	63.44	64.35	55.41
CaO	0.05	b.d.	0.10	0.10	0.91	0.99	0.21	0.86	0.29	0.29	0.23	0.88
CuO	0.39	0.52	0.52	0.27	0.24	0.23	1.40	b.d.	b.d.	b.d.	b.d.	b.d.
FeO	1.48	1.06	1.02	1.10	0.93	0.45	3.11	0.40	b.d.	b.d.	0.18	0.51
PbO	8.82	8.82	12.23	13.13	b.d.	2.44	20.98	1.40	1.61	1.30	1.53	8.58
SrO	b.d.	b.d.	b.d.	b.d.	1.62	0.99	b.d.	0.94	b.d.	b.d.	b.d.	0.67
Na_2O	b.d.	0.28	b.d.	b.d.	0.14	b.d.	b.d.	b.d.	b.d.	b.d.	0.18	b.d.
Sum	100.22	100.09	99.23	99.84	99.22	100.05	99.08	100.35	99.42	98.98	101.24	100.22
Ba^{2+} apfu	0.848	0.844	0.813	0.817	0.888	0.892	0.622	0.914	0.969	0.975	0.963	0.845
Ca^{2+}	0.002	0.000	0.004	0.004	0.037	0.040	0.009	0.035	0.012	0.012	0.009	0.037
Cu^{2+}	0.012	0.015	0.016	0.008	0.007	0.007	0.042	0.000	0.000	0.000	0.000	0.000
Fe^{2+}	0.048	0.035	0.034	0.037	0.029	0.014	0.103	0.013	0.000	0.000	0.006	0.017
Pb^{2+}	0.093	0.092	0.131	0.142	0.000	0.025	0.225	0.014	0.017	0.014	0.016	0.090
Sr^{2+}	0.000	0.000	0.000	0.000	0.035	0.022	0.000	0.021	0.000	0.000	0.000	0.015
Na^+	0.000	0.011	0.000	0.000	0.005	0.000	0.000	0.000	0.000	0.000	0.007	0.000
Catsum	1.003	0.996	0.998	1.008	1.001	1.000	1.002	0.996	0.998	1.001	1.001	1.003
S^{6+}	0.999	0.998	1.001	0.997	0.998	1.000	0.999	1.001	1.001	1.000	0.998	0.999
Ansum	0.999	0.998	1.001	0.997	0.998	1.000	0.999	1.001	1.001	1.000	0.998	0.999

5.3. Smelting Experiments

Series of experiments were performed to clarify approximate melting point of the slags. The results of individual tests are presented in Figure 8. The lowest testing temperature (1000 °C) resulted in the colour change of the samples to greenish-black, sometimes with a light red hue. Only the samples JS1 (swelling) and PL5 (bending) indicated signs of softening. The increase in temperature (1050 °C) led to the blackening of most samples and melting of edges of some of them. The first striking change in shape occurred at 1100 °C. The majority of Type A slags were liquid enough to form a bead; the outcome for the remaining samples was at least a glossy surface and melted edges. The Type B slags underwent minor deformation of the edges, except for sample CP1, which was partially melted. The exposure to temperature of 1150 °C resulted in flattening of most of the Type B slags with some difficulties for the Site 4 slags. The Type A slags were either flattened or bead-shaped. The highest testing temperature was followed by the complete melting of sample ML24. The samples PL3, PL7, PL10, JS9, and CP5 represent exceptions because they did not achieve sufficient flatness, even after exposure to the highest temperature.

Sample	PL3	PL5	PL7	PL10	ML2	ML3	ML7	ML24	ML25
Type	A	B	A	A	A	A	A	B	B
Site	1	1	1	1	2	2	2	2	2
Calculated liquidus (°C)	1154	1122	1164	1147	1183	1187	1182	1121	1084
1000 °C									
1050 °C									
1100 °C									
1150 °C									
1200 °C									
Sample	JS1	JS3	JS4	JS6	JS9	CP1	CP5	CP7	CP10
Type	B	B	B	B	B	B	B	B	B
Site	3	3	3	3	3	4	4	4	4
Calculated liquidus (°C)	1115	1075	1114	1139	1081	1093	1107	1105	1106
1000 °C									
1050 °C									
1100 °C									
1150 °C									
1200 °C									

Figure 8. Appearance of selected samples exposed to various temperature conditions.

6. Discussion

6.1. Origin of Barium-Rich Slags

While Pb-rich slags are a quite common phenomenon (e.g., [8,11]), high barium contents discovered in the JOD Type B slags are unique not only in the context of Czech Republic, but the whole of Europe. Relatively high contents of barium in slags are reported from the Harz Mountains (up to 6.0 wt.% of BaO by [42] and up to 9.3 wt.% of BaO by [41]), Wiesloch near Heidelberg (up to 10.1 wt.% of BaO; [9]) and indirectly from work of [47], dedicated mostly to secondary phases developed in slag heaps of Austrian Waitschach. Other localities, associated with Ba-rich slags, are in English Derbyshire, where large volumes of lead were produced in so-called bole furnaces. Unfortunately, only qualitative data are published so far; therefore, we can only assume high Ba contents

from the presence of Pb-Ca-Ba glass and relicts of unreacted baryte within slags [48]. Bole slags were derived from the smelting of crude galena ore without any pre-roasting procedures in low “furnaces” with oval or round base, resembling fire pit. That makes the medieval lead industry unusual in European context [2,48]. On a similar origin of Type B slags point out high barium and low iron contents and against are low S^{tot} (0.17–0.88 wt.%), As (6–71 ppm), Sb (2–103), and PbO (0.1–5.7 wt.%) contents. The low content of PbO is the key argument for a different method, because bole smelts were notoriously known for excessive loss of lead in slags, which were in later periods transported to black-work mills established near watercourses and reworked here or recycled in small-scale smelts on site [49]. The awareness of significant amount of lead in bole slags is apparent from its quantification and pricing in ledgers [50]. While the Type B slags from Sites 1 and 2 are relatively Pb-rich, a brief comparison between bulk and glass PbO contents together with extremely low S^{tot} contents (Figure 9) implicate that a part of the lead is present in its metallic form “frozen” within silicate matrix and not chemically bound into the glass itself, which reflects insufficient separation of reduced metal, rather than a flaw in smelt composition.

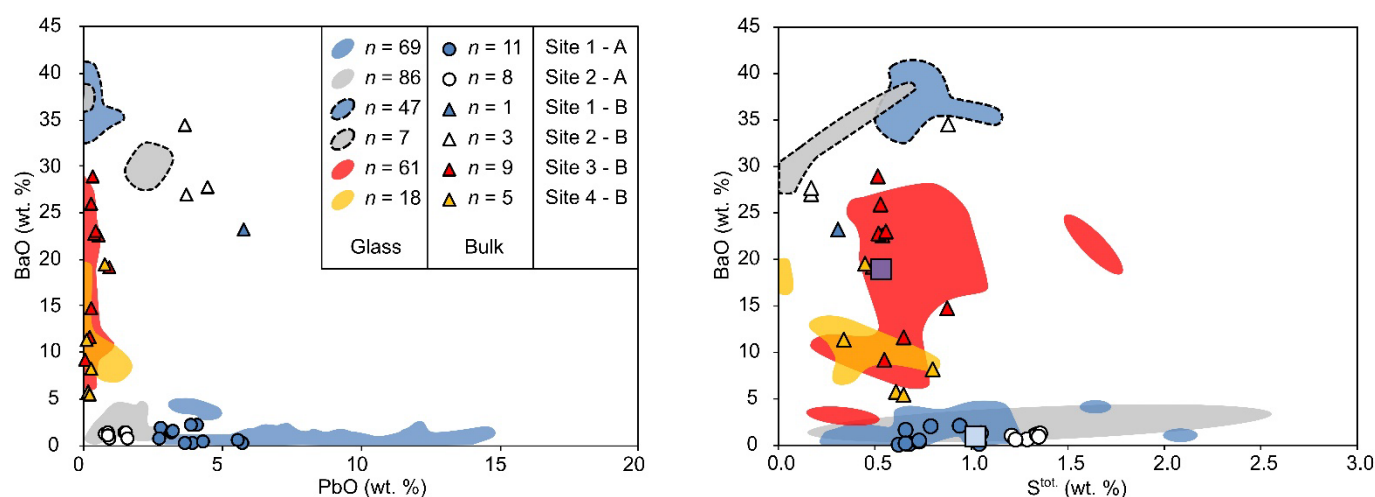


Figure 9. Selected bivariate plots of bulk and glass composition.

Certain analogy can be seen between Type B slags from Site 2 and wastes produced during cupellation. Cupellation is process of silver refining through forced lead oxidation. Slags related to this process are known for unusual mineralogical composition, namely by the presence of wollastonite, Pb analogue of larnite, Pb-rich melilites, and kalsilite and other rather exotic phases together with an excessive amount of glass [46,51]. Additionally, elevated contents of P_2O_5 (up to 1.4 wt.%) are common since bone ash was used for construction of furnace inner lining, responsible for litharge (PbO) absorption. On the other side, contents of SO_3 (usually less than 0.1 wt.%) and Zn (in the range of hundreds of ppm) are extremely low, because only lead bullions together with additives were processed [46]. Aside from the obviously high PbO contents in cupellation slags, the similarity can be seen in Site 2 slags due to their enrichment in P_2O_5 (up to 1.4 wt.%) followed by low contents of S^{tot} (as low as 0.2 wt.%) and Zn (1400–6000 ppm) as well as unusual phase composition dominated by glass. However, high barium contents do not align with the technology and any addition of baryte during the process is doubtful.

Another resemblance could be found in the ancient Chinese Pb-Ba-rich glass (~475BC–220 AD). The raw material for glass production was represented by a mixture of galena, witherite ($BaCO_3$), and quartz sand. The remaining elements in the composition are interpreted as impurities, except for Na and Cl, supposedly reflecting the addition of rock salt [52]. The glass served as a cheaper imitation of jade, for its dark green colour,

and only to a limited extent as household glassware, because of its low resistance to thermal shock [52,53]. However, the origin of Ba-rich slags in intentional glass production seems in the light of the archaeological context, together with the long-term tradition of wood ash lime glass production within Europe (uniform composition since the 13th century), to be questionable at least [54–56].

In spite of proposed options, the most relevant origin of Ba-rich slags could be seen in the main smelts, which were performed under reducing conditions. The evidence supporting the proposed theory, is based on the fact that on Site 2, both types of slag were sampled from the same layer and contents of silver (67 ppm in Type A and 79 ppm in Type B slags); other trace elements are, on average, very similar. Moreover, only strongly reducing conditions prevent the existence of otherwise common trivalent iron-bearing phases such as, e.g., magnetite. Additionally, the Jihlava Ore District was significantly influenced by German-speaking miners and metallurgists, migrating from iconic localities known for working baryum-rich gangue and producing Ba-rich slags related to Pb-Ag smelting [41]. Even [42] and [57] consider in their works the addition of baryte as a common phenomenon in medieval metallurgy of lead and silver. This hypothesis is reinforced in Czech archaeology by [58], which mentions baryte as an additive rather than waste or a non-separable component. Finally, a single small heap of baryte gangue unearthed during archaeological excavations at the SHD area nicely completes the whole picture [23]. The main role of barium in medieval metallurgy is attributed to the displacing of lead from silicate glass, resulting in a lower loss of the metal and thus improving process effectivity [58]. This opinion agrees with analytical data because the Type B slags are, on average, lead-poor when compared with Type A (Figure 9, Table 1). There are indeed some exceptions to the theory mentioned earlier; however, they might represent unfavourable temperature conditions rather than the error in concept. The addition of BaO is used for the dephosphorization and desulphurization of produced alloys in modern ferrous metallurgy [59].

The existence of baryte-rich gangue at Site 1 is not proven yet; therefore, the single finding of Ba-rich slags could be explained either by the transfer of ore/gangue from another mining site or the accidental finding of spatially small baryte-rich mineralization [22].

While Type B material from the JOD is geochemically similar to other localities regarding Ba-rich slags, there are some striking differences in phase composition. Specifically, in the Wiesloch slags, the bulk FeO contents are projected in the presence of fayalitic olivine, iscorite, and magnetite-enriched spinelide, as well as increased admixtures in leucite (up to 2.6 wt.% of Fe₂O₃) and feldspar (up to 4.9 wt.% Fe₂O₃). Similar trends apply also to Harz localities with the addition of hedenbergite-rich pyroxene [41] and Fe-rich melilite [42]. In Type B slags from the JOD, there are melilite and diopside-rich pyroxene (max. 20 mol.% Fs), the main Fe-bearing phases among silicates; however, they are only accessory, and their presence is restricted to samples JS5 (Mel + Px) and JS6 (Px). On the other hand, strongly zoned, Ba-rich feldspars are iconic for both the JOD and comparison sites (up to 31.8 wt.% of BaO in [9] and up to 26.8 wt.% of BaO in [42]).

6.2. Ore Processing and Composition of Charge

Heat was applied to the sulphidic ores multiple times through the whole process of silver release, starting with ore body softening during the mining campaign and ending with metal purification before the coins were minted [31]. However, the first step, which resulted in significant chemical alteration of the ore, is considered the roasting procedure in silver–lead metallurgy [60]. This activity allowed the removal sulphur as well as other volatile elements (e.g., As, Sb) from charge, reducing the amount of secondary formed speiss (mixture of metallic arsenides) or matte during smelting [31]. Nevertheless, part of sulphur was present in sulphates, which are capable to withstand temperatures achieved during roasting (not higher than 1000 °C) unless a low-melting component such as, for example, litharge is present [48]. The quality of the process is evaluated based on sulphur

contents with borderline being set to 1 wt.%. Values over 1 wt.% are interpreted as poorly roasted ore, and vice versa [61]. Therefore, Type B slags and a major portion of Type A slags from Site 1 reflect good roasting of the ore. The samples ML25, ML26, and PL5 could be even considered dead roasted, since the contents of S^{tot} are in 0.17–0.33 wt.% range. Surprisingly, there is no correlation between sulphur and baryum, neither on the level of bulk composition nor point glass analyses (Figure 9), despite the origin of high BaO contents in baryte [22]. In contrast, Type A slags from Site 2 were roasted poorly. However, the slags reflect a significantly better roasting routine than samples from the nearby Kutná Hora Ore district (slags from 14–15th century), where contents of S^{tot} are between 3.0 and 5.0 wt.% [6]. On the other hand, slags from the Příbram Ore District, dated back to the 13th century, yielded, with one exception (0.9 wt.% of S^{tot}), far better results (0.1–0.4 wt.% of S^{tot}) [8]. Such low sulphur contents are typical for slags related to carbonate rather than sulfidic-based mineralization (averages 0.1–0.5 wt.% of S^{tot} [12]).

The K_2O contents are slightly above average when compared with other medieval smelting localities within Europe (e.g., 0.9–1.8 wt.%; [9]); however, they are significantly lower than in similar material dated to the 18th century (3.4–6.7 wt.%; [10]). The source of K is by many authors seen in potash or partial anatexis of K-rich host rocks used for furnace construction (e.g., [9]). While the Moldanubian Zone is known for the presence of high-potassic durbachites, the closest ore body of such a composition is the Jihlava Pluton (with up to 6.9 wt.% of K_2O), which is approximately 5 km away [62]. The local gneisses, migmatites, and granites yield similar K_2O contents in the range of 4.7–5.8 wt.% [63,64]. Feldspars and micas, the main carriers of K in silicate rocks, are released upon weathering and become part of the local soils. The affection of the slags' K_2O contents solely by partial melting of rocks or loam could be ruled out based on the K/Na ratio, which is in significantly higher slags (on average 4.6 for Type A slags and 4.2 for Type B slags), pointing to the source of alkalis in both charcoal (birch 18, beech 13, oak 18; [65]) and local rocks (1.3–2.2 migmatites, 1.5–2.1 two-mica granites, 3.0 durbachite from the Jihlava Pluton, and 1.7–2.6 soil on migmatites) [62,64,66]. The positive correlation between K_2O and Al_2O_3 contents in slags is particularly interesting, because both elements could be derived from multiple sources (potash, loam, ore, rocks, or other additives). Since the Al/K ratio is relatively constant, it seems that the final Al_2O_3 content is controlled by potassium input. The elevated contents of K_2O and Al_2O_3 for Type A slags from Site 1 could therefore be interpreted as higher fuel consumption, but not necessarily resulting from higher smelting temperatures, as verified by liquidus calculations, and smelting experiments (see Table 7).

Table 7. Estimation of smelting temperatures (°C) for individual slag types and sites based on ternary diagrams, liquidus calculations and experimental smelts. The glass liquidus is derived from average values for samples. Av—average value, #—maximum temperature did not result in satisfactory melting of all samples, CaO^* —($CaO + BaO + Al_2O_3$), FeO^* — $FeO + ZnO + MnO$).

Type	A	B	A	B	B	B
Site	1	1	2	2	3	4
SiO ₂ -CaO-FeO	1600–1700	1700	1550–1600	~1700	~1700	~1700
SiO ₂ -CaO*-FeO*	1100–1600	1400	1150–1300	~1500	1250–1500	1400–1600
SiO ₂ -Al ₂ O ₃ -FeO	1400–1500	1500	1400–1470	~1500	1550–1590	~1580
SiO ₂ -Al ₂ O ₃ -BaO	1600–1700	1300	~1650	~1250	1250–1450	1400–1500
bulk liquidus	1147–1260	1122	1182–1191	1084–1121	1075–1152	1093–1107
glass liquidus	1068–1158	1101	1129–1173	1081–1142	1088–1172	1091–1137
bulk liquidus (Av)	1173	1122	1186	1098	1119	1101
glass liquidus (Av)	1106	1101	1146	1114	1117	1111
experimental smelts	1150–1200 #	1150	1150	1150–1200	1150–1200 #	1150–1200 #

The presence of quartz in slags is at least partly proof of non-equilibrium smelting conditions related either to insufficient smelting temperature or short holding time of slag

in a furnace [1,8] (and references there in). Quartz fused into a bottom of a sample might also be a result of manipulation with semi-solidified slag outside the furnace. The authors of [31] mentioned different tooling, namely, hooks, and bars for slag removal from fore-heart. It was carried out before the underlying layers of matte, speiss (if present), and lead bullion solidified, as can be interpreted from ripples on presumed molten metallic compound in the illustrations from Agricola's manuscript. The existence of quartz-rich layer underneath the upper surface of a slag might be, in fact, intentional. According to [2], the surface of molten slag was sprinkled with quartz sand to raise slag viscosity, which simplified its extraction in a semi-solidified state. The next step, represented by quenching, could be considered for Type A slags from Site 2 due to the coexistence of two morphologically different generations of olivine crystals and the absence of feldspar, which should otherwise (according to Melts software) form under 910–950 °C [39].

The contents of BaO and MnO play important role in ore type identification. It is possible to link Type A slags from Site 1 with the widespread ore type composed of Mn-rich carbonate gangue [22]. The high MnO contents are in slags incorporated in glass and Fe-bearing silicates such as olivine and pyroxene. The same also applies to elevated ZnO contents. The ZnO contents are significantly lower in slags at the remaining sites, although the mined mineralization was rich in sphalerite [22]. Zinc was an unwanted element in running smelt for its low boiling point. The escaping zinc fumes quickly condensed in higher parts of furnaces and therefore decreased the effective cross-section of construction. This phenomenon was described as the freezing of furnaces [31]. Thus, one explanation of low zinc contents might be in separation of sphalerite from charge, the second in boiling of most of the zinc during smelting. The second option requires strongly reducing conditions; otherwise, zinc is present as an oxide with a boiling point of 2360 °C [13,42]. The conditions for zinc boiling were probably met at least for the Type A slags from Site 2, since they contain reduced iron within metallic inclusions.

High BaO contents in Type B slags are with one exception (sample PL5) in spatial connection with baryte-rich mineralization. Baryte bearing mineralization is impoverished in carbonates [22], which is in the context of elevated contents of CaO surprising. However, the amount of CaO in slags is in comparison with foreign localities on average lower (e.g., [4,5,8,13]). The CaO contents in Type A slags are comparable with the results (1.6–6.9 wt.% of CaO) presented in the work of [41] from Harz Mountains. Similar contents (0.5–5.3 wt.% of CaO in Pb-rich slags) are among domestic localities reported from Příbram Ore District [8]. The slags from Kutná Hora Ore District yielded values between 3.8–18.2 wt.% of CaO [6]. Despite the low contents of CaO, phases such as pyroxene and anorthite-rich feldspar are present in Type A slags.

6.3. The Smelting Temperature and Efficiency of Metal Recovery

The estimations of smelting temperatures are for European medieval furnaces with forced draft in the range of 1100–1300 °C [61]. Even English boles, which worked on principal of natural draft, were able to achieve temperatures as high as 1000 °C [49]. Different ternary plots are widely used for approximation of smelting temperatures, but the obtained values are with minor exceptions considered as the absolute maximum, since only limited components are considered [8–10]. The plots may in fact yield unrealistic conditions at least for medieval metallurgy [10], as seen from the example of SiO₂-CaO-FeO system which gives temperature in the range of 1550–1700 °C (Figure 10). On the other hand, the modified plot SiO₂-CaO*-FeO* gives for Type A slags more reasonable values (1100–1600 °C for Site 1 and 1150–1300 °C for Site 2), because ZnO + MnO and BaO + Al₂O₃ contents are added to FeO and CaO components, respectively [42]. Similarly, the system SiO₂-Al₂O₃-BaO yields lower temperature conditions for Type B slags. The temperature range derived from SiO₂-Al₂O₃-FeO is relatively uniform; however, it is high for all analysed slags (1400–1590 °C).

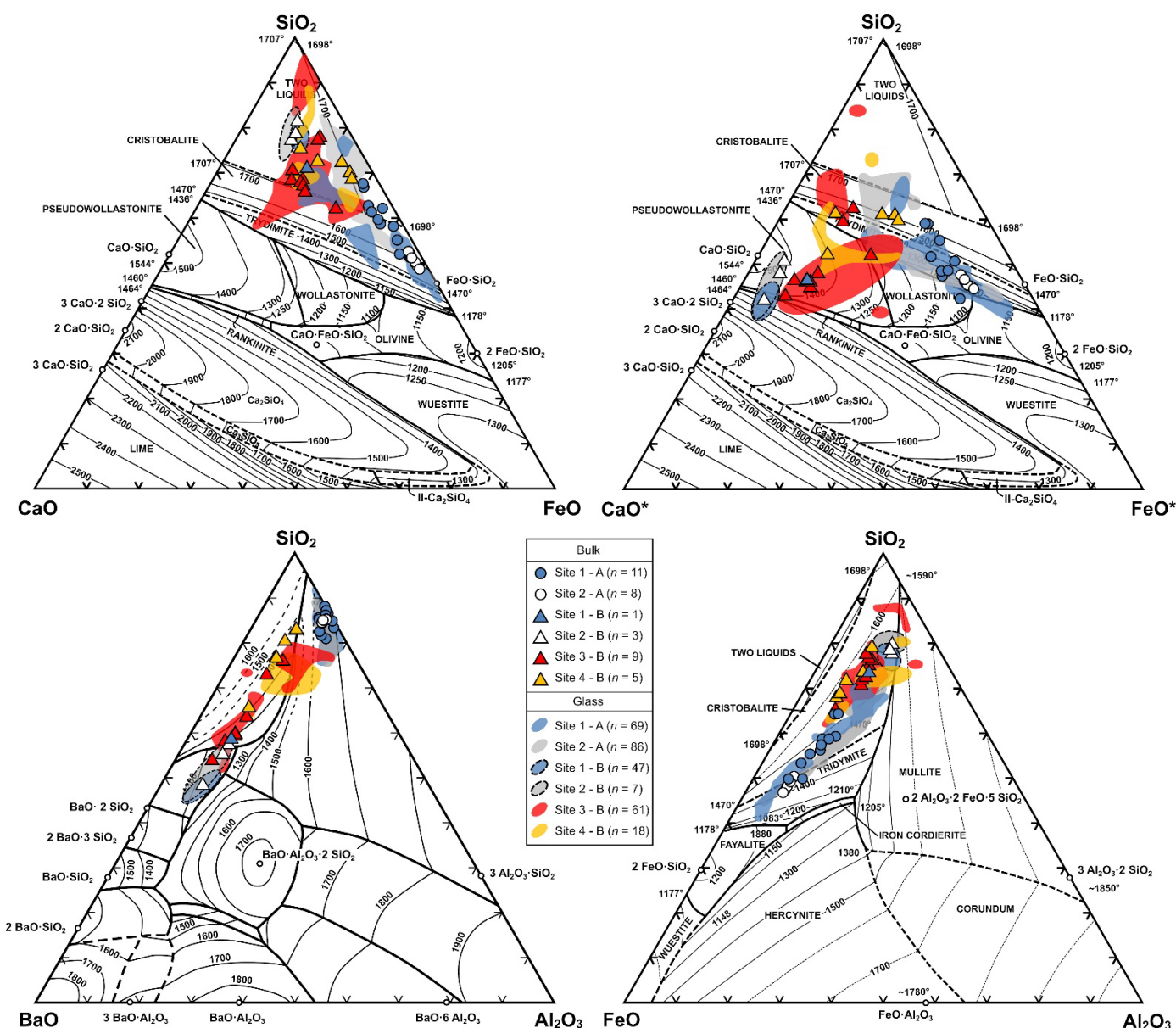


Figure 10. The smelting temperatures derived from ternary plots. System SiO₂-CaO-FeO and SiO₂-FeO-Al₂O₃ according to [67], system SiO₂-CaO*-FeO* according to [42], and system SiO₂-BaO-Al₂O₃ according to [68]. CaO*—(CaO + BaO + Al₂O₃), FeO*—(FeO + ZnO + MnO).

The calculated liquidus (Table 7) yields similar values for the same slag types (averages 1173 °C and 1186 °C for Type A slags and 1098 °C, 1101 °C, 1119 °C, and 1122 °C for Type B slags). The results are, with minor exceptions [40,41], comparable to other Czech and European localities (Table 8), and they are also relatively consistent with experimental observations. However, the application gives slightly underestimated values for Type B slags because it was developed for common rocks and therefore it does not account for high BaO contents [39]. The liquidus calculated from spot analyses is similar to bulk values, since the Type B slags are composed mostly of glass (e.g., average 1119 °C for bulk and 1117 °C for glass from Site 3). On the other hand, Type A slags yield lower temperatures for glass (average 1106 °C for Site 1 and 1146 °C for Site 2) than for bulk (average 1173 °C for Site 1 and 1186 °C for Site 2). Among the recent studies, [10] reports similar liquidus calculations in the range of 1200–1250 °C for 18th century Polish slags with exceptions for the younger site, which gives 1350–1450 °C. Similarly, the authors mention an approximate 60 °C difference between the results obtained from bulk and glass

composition. In our case, the difference was also verified during experimental smelts. The interstitial glass is, among other elements (e.g., PbO), enriched in alkalis, especially in samples lacking feldspars; therefore, the glass softens and melts under lower temperatures. However, the presence of crystalline phases makes the change in shape gradual. In contrast, the glass-dominated slags melt abruptly in a narrow temperature window unless they are enriched in quartz. The presented temperatures should be considered as the smelting minimum with questionable metal separation efficiency (e.g., samples ML24, ML25, PL5). Any increment in temperature would lead to the lowering of melt viscosity and better slag–metal liquation and gravitational separation [1,60]. It means that Type B slags with slightly lower densities are advantageous (average 3.07 g/cm³ for Type B slags and 3.27 g/cm³ for Type A slags).

Melt viscosity could be estimated from ternary plots [42] or calculated from bulk/glass composition [1]. Various computations of viscosity indexes were proposed for broad estimation of metal recovery efficiency with borderline being set to v.i. = 1 (e.g., [1,8]). The average values are in the range of 0.4–3.3 for European [61] and 0.6–1.2 for Czech localities [6,8,46]. In our study, the bulk compositions of Type A (v.i. = 0.8, v.i.mod = 0.9) and B (v.i. = 0.8, v.i.mod = 0.8) slags yield almost identical averages of viscosity indexes and the spot analysis of glass give more favourable results for Type B (average v.i. = 0.7–1.0, v.i.mod = 0.7–1.1) than Type A slags (average v.i. = 0.6–0.7, v.i.mod = 0.6–0.9). Therefore, the efficiency of metal extraction could be, based on the presented data, evaluated for most of the samples as medium to high with some silica-rich exceptions (e.g., JS9) falling into the category of unsatisfactory.

Table 8. Estimation of smelting temperatures (°C) for different European localities based on ternary diagrams and liquidus calculations. Av—average value, comparative data: 1*—Czech Republic [8], 2*—Germany [9], 3*—Czech Republic [6], 4*—Germany [40], 5*—Germany [41], 6*—Germany [42].

	1*	2*	3*	4*	5*	6*
Location	Příbram	Wiesloch	Kutná Hora	Harz	Harz	Harz
SiO ₂ -CaO-FeO	1300–1700	1110–1600	1150–1300	1175–1600	1125–1500	1175–1700
SiO ₂ -CaO*-FeO*	1300–1700	1100–1200	1125–1200	1150–1200	1100–1250	1150–1450
SiO ₂ -Al ₂ O ₃ -FeO	1400–1600	1180–1500	1300–1400	1180–1470	1150–1400	1200–1550
SiO ₂ -Al ₂ O ₃ -BaO	1600–1700	1300–1700	1600–1700	1650–1700	1350–1700	1550
bulk liquidus	1127–1438	1094–1403	1040–1307	1149–1661	1179–1540	1164–1300
bulk liquidus (Av)	1171	1237	1194	1355	1393	1211

7. Conclusions

The study of metallurgical wastes from the Jihlava Ore District resulted in the discovery of two chemical and mineralogical different groups of slags. The first group is rich in baryum, and the second represents fayalitic slags, locally enriched in MnO and ZnO. Both types of slags were linked to the same step in metallurgy of Pb-Ag, based on geochemical similarities and archaeological context. While there is a noticeable difference in composition, the observed/calculated melting temperatures (~1100–1200 °C) as well as calculated viscosity indexes are not only comparable, but in many cases, the same for both types of slag. Nevertheless, the Ba-rich samples seem to be more advantageous (with some exceptions) for lower lead losses at similar or even lower fuel consumption, as seen from lower K₂O and Al₂O₃ contents. The quality of the roasting procedure is, on average, better for Type B slags. It seems that the charge was at least partially self-fluxing with fluxes derived from gangue (quartz, Mn-rich carbonates, and baryte) and host rocks with possible minor input of CaO-rich additive in the case of Type B slags. At the very least, Type A slags from Site 2 bear signs of manipulation in a semi-solidified state and intentional increase in surface viscosity followed by quenching. Thanks to the chemical contrast in the

composition of gangue of local mineralization, it is possible to link the slags to their respective sources and even suggest a possibility of transfer of material between localities.

Author Contributions: Conceptualization, J.K., Z.D., O.S. and K.M.; methodology, J.K. and Z.D.; software, J.K.; validation, Z.D., O.S. and K.M.; formal analysis, J.K. and Z.D.; investigation, J.K. and Z.D.; resources, J.K. and Z.D.; writing—original draft preparation, J.K.; writing—review and editing, J.K., Z.D., O.S. and K.M. All authors have read and agreed to the published version of the manuscript.

Funding: Part of this research was funded by the Ministry of Culture of the Czech Republic (long-term project DKRVO 2019-2023/1.III.d, 00023272).

Data Availability Statement: All representative data are contained in this work.

Acknowledgments: Part of the analytical work was supported by the Ministry of Culture of the Czech Republic, project NAKI II DG20P02OVV007.

Conflicts of Interest: The authors declare no conflict of interest.

References

- Bachmann, H.G. *The Identification of Slags from Archeological Sites*; Routledge: London, UK, 1988.
- Tylecote, R.F. *A History of Metallurgy*, 2nd ed.; Maney Publishing: London, UK, 1992.
- Gong, W.; Chen, Q.; Miao, J. Bond behaviors between copper slag concrete and corroded steel bar after exposure to high temperature. *J. Build. Eng.* **2021**, *44*, 1–13. <https://doi.org/10.1016/j.job.2021.103312>.
- Manasse, A.; Mellini, M.; Viti, C. The copper slags of the Capattoli Valley, Campiglia Marittima, Italy. *Eur. J. Mineral.* **2001**, *13*, 949–960. <https://doi.org/10.1127/0935-1221/2001/0013/0949>.
- Manasse, A.; Mellini, M. Chemical and textural characterisation of medieval slags from the Massa Marittima smelting sites (Tuscany, Italy). *J. Cult. Herit.* **2002**, *3*, 187–198. [https://doi.org/10.1016/S1296-2074\(02\)01176-7](https://doi.org/10.1016/S1296-2074(02)01176-7).
- Manasse, A.; Mellini, M. Archaeometallurgic slags from Kutná Hora. *Neues Jahrb. für Mineral. Monatshefte* **2002**, *8*, 369–384. <https://doi.org/10.1127/0028-3649/2002/2002-0369>.
- Sáez, R.; Nocete, F.; Nieto, J.M.; Capitán, M.Á.; Rovira, S. The extractive metallurgy of copper from Cabezo Juré, Huelva, Spain: Chemical and mineralogical study of slags dated to the third millenium B.C. *Can. Mineral.* **2003**, *44*, 627–638. <https://doi.org/10.2113/gscanmin.41.3.627>.
- Ettler, V.; Červinka, R.; Johan, Z. Mineralogy of medieval slags from lead and silver smelting (Bohutín, Příbram District, Czech Republic): Toward estimation of historical smelting conditions. *Archaeometry* **2009**, *51*, 987–1007. <https://doi.org/10.1111/j.1475-4754.2008.00455.x>.
- Ströbele, F.; Wenzel, T.; Kronz, A.; Hildebrandt, H.; Markl, G. Mineralogical and geochemical characterization of high-medieval lead-silver smelting slags from Wiesloch near Heidelberg (Germany)—An approach to process reconstruction. *Archaeol. Anthropol. Sci.* **2010**, *2*, 191–215. <https://doi.org/10.1007/s12520-010-0039-7>.
- Kądziołka, K.; Pietranik, A.; Kierczak, J.; Potysz, A.; Stolarczyk, T. Towards better reconstruction of smelting temperatures: Methodological review and the case of historical K-rich Cu-slags from the Old Copper Basin, Poland. *J. Archaeol. Sci.* **2020**, *118*, 1–19. <https://doi.org/10.1016/j.jas.2020.105142>.
- Cabała, J.; Warchulski, R.; Rozmus, D.; Środek, D.; Szełęg, E. Pb-rich slags, minerals, and pollution resulted from a Medieval Ag-Pb smelting and mining operation in the Silesian-Cracowian region (southern Poland). *Minerals* **2020**, *10*, 28. <https://doi.org/10.3390/min10010028>.
- Derkowska, K.; Świerk, M.; Nowak, K. Reconstruction of Copper smelting technology based on 18-20th-century slag remains from the Old Copper Basin, Poland. *Minerals* **2021**, *11*, 926. <https://doi.org/10.3390/min11090926>.
- Warchulski, R.; Szczuka, M.; Kupczak, K. Reconstruction of 16th–17th century lead smelting processes on the basis of slag properties: A case study from Sławków, Poland. *Minerals* **2020**, *10*, 1039. <https://doi.org/10.3390/min10111039>.
- Ash, C.; Borůvka, L.; Tejnecký, V.; Nikodem, A.; Šebek, O.; Drábek, O. Potentially toxic element distribution in soils from the Ag-smelting slag of Kutná Hora (Czech Republic): Descriptive and prediction analyses. *J. Geochem. Explor.* **2013**, *144*, 328–336. <https://doi.org/10.1016/j.gexplo.2013.11.010>.
- Ettler, V.; Johan, Z. 12 years of leaching of contaminants from Pb smelter slags: Geochemical/mineralogical controls and slag recycling potential. *Appl. Geochem.* **2014**, *40*, 97–103. <https://doi.org/10.1016/j.apgeochem.2013.11.001>.
- Yin, N.H.; Sivry, Y.; Avril, C.; Borensztajn, S.; Labanowski, J.; Malavergne, V.; Lens, P.N.L.; Rossano, S.; Hullebusch, E.D. Bio-weathering of lead blast furnace metallurgical slags by *Pseudomonas aeruginosa*. *Int. Biodeterior. Biodegrad.* **2014**, *86*, 372–381. <https://doi.org/10.1016/j.ibiod.2013.10.013>.
- Tyszka, R.; Kierczak, J.; Pietranik, A.; Ettler, V.; Mihaljevič, M. Extensive weathering of zinc smelting slag in a heap in Upper Silesia (Poland): Potential environmental risks posed by mechanical disturbance of slag deposits. *Appl. Geochem.* **2014**, *40*, 70–81. <https://doi.org/10.1016/j.apgeochem.2013.10.010>.

18. Potysz, A.; Kierczak, J.; Pietranik, A.; Kądziołka, K. Mineralogical, geochemical, and leaching study of historical Cu-slugs issued from processing of the Zechstein formation (Old Copper Basin, southwestern Poland). *Appl. Geochem.* **2018**, *98*, 22–35. <https://doi.org/10.1016/j.apgeochem.2018.08.027>.
19. Derner, K.; Hrubý, P.; Malina, O.; Večeřa, J. Hornické revíry vrcholného středověku a raného novověku ve srovnávacím pohledu—Mining regions in the high Middle Ages and the early modern age viewed in terms of comparison. *Archaeol. Hist.* **2019**, *44*, 925–947.
20. Derner, K.; Hrubý, P. Farming and food production in medieval mining communities. *Archaeol. Hist.* **2018**, *43*, 207–239. (In Czech)
21. Hrubý, P.; Hejhal, P.; Kočár, P.; Libor, P.; Malý, K. *Central Bohemian-Moravian Highlands on the Threshold of the High Middle Ages Archaeology, Geochemistry and the Analyses of Alluvial Sediments*; Opera Universitatis Masarykianae Brunensis, Facultas Philosophica. Masarykova univerzita: Brno, Czech Republic, 2014, p. 266. (In Czech)
22. Pluskal, O.; Vosáhlo, J. Jihlavský rudní obvod. *Vlastivěd. sb. Vysoč.* **1988**, *13*, 157–191. (In Czech)
23. Hrubý, P. Středověká hornická aglomerace na Starých Horách u Jihlavy. *Stříbrná Jihlava* **2004**, 5–21. (In Czech)
24. Zajíček, P. Evaluation of Ag reserves in the Jihlava ore district. *Čas. Mineral. Geol.* **1983**, *28*, 197–207. (In Czech)
25. Bernard, J.H. *Empirical Types of Ore Mineralizations in the Bohemian Massif*; Geological Survey: Prague, Czech Republic, 1991.
26. Koutek, J. O rudních žilách a starém dolování u Jihlavy. *Sbor. Ústř. Úst. Geol. Odd. Geol.* **1952**, *19*, 77–116. (In Czech)
27. Němec, D. Geologische und paragenetische Verhältnisse der Erzgänge des Jihlava-Jezdovicer Reviers. *Tschermaks Mineral. Petrogr. Mitt.* **1964**, *9*, 42–85. (In German).
28. Malý, K. Chemistry of carbonates from Jihlava Ore District. *Acta Rer. Natur. Přír. Čas. Vysočiny* **2009**, *7*, 57–62. (In Czech)
29. Malý, K.; Dolníček, Z. Pb-Zn-Ag vein mineralization of central part of the Českomoravská vrchovina Upland (Czech Republic): S, C and O stable isotope study. *Bull. Geosci.* **2005**, *80*, 307–319.
30. Hrubý, P. *Metalurgická Produkční Sféra a Neagrární Sídlní Struktura v Závěru Přemyslovské Éry na Centrální Českomoravské Vrchovině*. Habilitation Thesis, Masaryk University, Brno, May 2017. (In Czech)
31. Hoover, H.C.; Hoover, I.H. *Georgius Agricola de Re Metallica*; Dover Publications: New York, NY, USA, 1950.
32. Hrubý, P. From Crude Silver to Coins, or from Smelters to Mints *Archaeol. Hist.* **2015**, *39*, 609–637. (In Czech)
33. Malý, K.; Vilímek, L.; Vokáč, M.; Zimola, D. Mining Settlement Evidence in the Alluvial Plain of the Bělokamenský Creek. *Archeol. Výzk. Vysoč.* **2007**, *1*, 125–144. (In Czech)
34. Šamalová, E. Defunct medieval metallurgical site near Jihlava. *Stříbrná Jihlava* **2007**, 228–237. (In Czech)
35. Havlíček, J. The Discovery of Ore Millstone Fragments Near the Metallurgy Plant in Plandry. *Archeol. Výzk. Vysoč.* **2015**, *4*, 170–172. (In Czech)
36. Hrubý, P.; Hejhal, P.; Malý, K. Těžba a úprava rudy na Jihlavských Starých Horách ve 13. století (Montánní archeologický výzkum a aplikace přírodovědných analýz). *Stříbrná Jihlava* **2007**, 238–269. (In Czech)
37. Zimola, D. Analýza keramických artefaktů ze Starých Hor u Jihlavy. *Acta Rer. Natur. Přír. Čas. Vysočiny* **2014**, *16*, 121–143. (In Czech)
38. Crkal, J.; Derner, K.; Hrubý, P.; Milo, P. Architecture of mining settlements in the late Přemyslid era. *Archaeol. Hist.* **2019**, *44*, 887–923. (In Czech)
39. Gualda, G.A.R.; Ghiorso, M.S. MELTS_Excel: A Microsoft Excel-based MELTS interface for research and teaching of magma properties and evolution. *Geochem. Geophys. Geosyst.* **2015**, *16*, 315–324. <https://doi.org/10.1002/2014GC005545>.
40. Eggers, T.; Ruppert, H.; Kronz, A. Change of copper smelting techniques during medieval times in the Harz-Mountains (Germany). In *Applied Mineralogy*; Rammlmair, D., Mederer, J., Oberthür, T., Heimann, R.B., Pentlinghaus, H., Eds.; Balkema: Rotterdam, The Netherlands, 2000, Volume 5; pp. 971–974.
41. Asmus, B. *Medieval Copper Smelting in the Harz Mountains, Germany*; Deutsches Bergbau-Museum: Bochum, Germany, 2012.
42. Chaudhuri, J.N.B.; Newesely, H. Mineralogical characterization of old Harz Mountain slags. *Can. Metall. Q.* **1993**, *32*, 1–12. <https://doi.org/10.1179/cm.1993.32.1.1>.
43. Ettler, V.; Johan, Z.; Vítková, M.; Skála, R.; Kotrlý, M.; Habler, G.; Klementová, M. Reliability of chemical microanalyses for solid waste materials. *J. Hazard. Mater.* **2012**, *221–222*, 298–302. <https://doi.org/10.1016/j.jhazmat.2012.04.015>.
44. Ettler, V.; Legendre, O.; Bodéan, F.; Touray, J.C. Primary phase and natural weathering of old lead-zinc pyrometallurgical slag from Příbram, Czech Republic. *Can. Mineral.* **2001**, *39*, 873–888. <https://doi.org/10.2113/gscanmin.39.3.873>.
45. Morimoto, N. Nomenclature of pyroxenes. *Am. Mineral.* **1988**, *73*, 1123–1133.
46. Ettler, V.; Johan, Z.; Zavřel, J.; Wallisová, M.S.; Mihaljevič, M.; Šebek, O. Slag remains from the Na Slupi site (Prague, Czech Republic): Evidence for early medieval non-ferrous metal smelting. *J. Archaeol. Sci.* **2015**, *53*, 72–83. <https://doi.org/10.1016/j.jas.2014.10.007>.
47. Kolitsch, U.; Brandstätter, F.; Schreiber, F.; Fink, R.; Auer, C. Die Mineralogie der weltweit einzigartigen Schlacken von Waitschach, Kärnten. *Ann. Naturhist. Mus. Wien Serie A* **2013**, *115*, 19–87. (In German).
48. Smith, R. A typology of lead-bale slags based on their physico-chemical properties. *Hist. Metall.* **2006**, *40*, 115–128.
49. Hamilton, K.; McDonnell, J.G.; Schmidt, A. Assessment of early lead working sites in the Yorkshire Dales by geophysical prospecting. *British Mining* **1999**, *63*, 156–164.
50. Kiernan, D.T. *The Derbyshire Lead Industry in the Sixteenth Century*; Derbyshire Record Society: Chesterfield, UK, 1989.
51. Zori, C.; Tropper, P. Silver lining: Evidence for Inka silver refining in northern Chile. *J. Archaeol. Sci.* **2013**, *40*, 3282–3292. <https://doi.org/10.1016/j.jas.2013.03.020>.

52. Qin, Y.; Wang, Y.; Chen, X.; Li, H.; Xu, Y.; Li, X. The research of burning ancient Chinese lead-barium glass by using mineral raw materials. *J. Cult. Herit.* **2016**, *21*, 796–801. <https://doi.org/10.1016/j.culher.2016.04.003>.
53. Cui, J.; Wu, X.; Huang, B. Chemical and lead isotope analysis of some lead-barium glass wares from the Warring States Period, unearthed from Chu tombs in Changed City, Hunan Province, China. *J. Archaeol. Sci.* **2011**, *38*, 1671–1679. <https://doi.org/10.1016/j.jas.2011.02.034>.
54. Wedepohl, K.H.; Simon, K. The chemical composition of medieval wood ash glass from Central Europe. *Geochemistry* **2010**, *70*, 1, 89–97. <https://doi.org/10.1016/j.chemer.2009.12.006>.
55. Pánová, K.; Rohanová, D.; Randáková, S. Modelling of Bohemian and Moravian glass recipes from Gothic to Baroque periods. *Herit. Sci.* **2020**, *117*, 1–12. <https://doi.org/10.1186/s40494-020-00459-z>.
56. Pánová, K.; Jílková, K.; Rohanová, D.; Lahodný, F.; Galusková, D.; Míka, M. Melting Process and Viscosity of Bohemian Historical Glasses Studied on Model Glasses. *Minerals* **2021**, *11*, 829. <https://doi.org/10.3390/min11080829>.
57. Scheinert, M.; Kupsch, H.; Bletz, B. Geochemical investigations of slags from the historical smelting in Freiberg, Erzgebirge (Germany). *Chem. Erde* **2009**, *69*, 81–90. <https://doi.org/10.1016/j.chemer.2008.03.001>.
58. Nováček, K. The mineral resources of medieval Bohemia as an archaeological problem: The state and perspectives of research into metal production and working. *Archeol. Rozhl.* **2001**, *53*, 279–309. (In Czech)
59. Sano, N. Thermodynamics of BaO bearing fluxes. In Proceedings of the 4th International Conference on Molten Slags and Fluxes, Sendai, Japan, 8–11 June 1992.
60. Vaněk, V.; Velebil, D. Early Metallurgy of silver. *Stříbrná Jihlava* **2007**, 188–205. (In Czech)
61. Kierczak, J.; Pietranik, A. Mineralogy and composition of historical Cu slags from the Rudawy Janowickie Mountains, south-western Poland. *Can. Mineral.* **2011**, *49*, 1281–1296. <https://doi.org/10.3749/canmin.49.5.1281>.
62. Kotková, J.; Schaltegger, U.; Leichmann, J. Two types of ultrapotassic plutonic rocks in the Bohemian Massif—Coeval intrusions at different crustal levels. *Lithos* **2010**, *115*, 163–176. <https://doi.org/10.1016/j.lithos.2009.11.016>.
63. René, M. Evolution of two mica granites in the area between Mrákotín and Řásná. *Geol. Res. Morav. Silesia* **2000**, *8*, 82–84. (In Czech)
64. Buriánek, D.; Soukup, M.; Ivanov, M. Migration of alkali metals in the weathering profiles of migmatites from the Svratka Crystalline Unit and Moldanubicum. *Geol. Res. Morav. Silesia* **2020**, *27*, 88–97. (In Czech)
65. Joosten, I. *Technology of Early Historical Iron Production in The Netherlands*; Institute for Geo- and Bioarchaeology: Vrije Universiteit Amsterdam, The Netherlands, 2004.
66. Breiter, K.; Scharbert, S. Two-mica and biotite granites in the Weitra-Nové Hradý area, Austria—Czech Republic. *J. Czech Geol. Soc.* **2006**, *51*, 3–4, 217–230. <https://doi.org/10.3190/JCGS.995>.
67. Muan, A.; Osborn, E.F. *Phase Equilibria among Oxides in Steelmaking*; Addison-Wesley Publishing Company, Inc.: Boston, MA, USA, 1965.
68. Hall, F.P.; Insley, H. *Phase Diagrams for Ceramists*; The American Ceramic Society Inc.: Columbus, OH, USA, 1947.